APPLICATIONS OF THE OSMIUM ISOTOPIC SYSTEM AND RHENIUM-PLATINUM GROUP ELEMENT CONCENTRATIONS IN ORGANIC-RICH MUD ROCKS FROM THE EAGLE FORD FORMATION, TEXAS: A GEOCHEMISTRY AND REDOX STUDY

A Thesis Presented to
the Faculty of the Department of Earth and Atmospheric Sciences
University of Houston

In Partial Fulfillment
of the Requirements for the Degree
Master of Science

By
Daniel Louis Sullivan
May 2017

APPLICATIONS OF THE OSMIUM ISOTOPIC SYSTEM AND RHENIUM- PLATINUM GROUP ELEMENT CONCENTRATIONS IN ORGANIC-RICH MUD ROCKS FROM THE EAGLE FORD FORMATION, TEXAS: A GEOCHEMISTRY AND REDOX STUDY

_____

Dan Sullivan

APPROVED:

_____

Dr. Alan Brandon, Chairman

_____

Dr. Qi Fu

_____

Dr. Steven Bergman

_____

Dean, College of Natural Sciences and Mathematics

"True scientific discovery renders the brain incapable at such moments of shouting vigorously to the world 'Look at what I've done! Now I will reap the benefits of recognition and wealth.' Instead such discovery instinctively forces the brain to thunder 'We did it' in a voice no one else can hear, within its sacred, but lonely, chapel of scientific thought.

— Clair Cameron Patterson, reacting to being the first person to discover the age of the earth.

"I believe in intuition and inspiration. Imagination is more important than knowledge. For knowledge is limited, whereas imagination embraces the entire world, stimulating progress, giving birth to evolution. It is, strictly speaking, a real factor in scientific research."

-Albert Einstein

"The craftsman who wishes to do his work well must first sharpen his tools."

-The Analects

"Be one with the beam."

-Alan Bandon

APPLICATIONS OF THE OSMIUM ISOTOPIC SYSTEM AND RHENIUM-PLATINUM GROUP ELEMENT CONCENTRATIONS IN ORGANIC-RICH MUD ROCKS FROM THE EAGLE FORD FORMATION, TEXAS: A GEOCHEMISTRY AND REDOX STUDY

An Abstract of a Thesis
Presented to
the Faculty of the Department of Earth and Atmospheric Sciences
University of Houston

In Partial Fulfillment
of the Requirements for the Degree
Master of Science

By
Daniel Louis Sullivan
May 2017

ABSTRACT

The concentration of Re and platinum group elements (Re-PGE) and $^{187}Os/^{188}Os$ ratios have been measured from ocean anoxic event 2 (OAE 2; ~94.87 - ~93.92 Ma) sediments from a West Texas core. The paleo-location of the core is the Comanche shelf near the southern mouth of the Cretaceous Western Interior Seaway (KWIS). Osmium geochemical data indicates a massive input of unradiogenic material to the oceans immediately before the onset of OAE 2. During OAE 2, two additional pulses of unradiogenic Os entered the oceans. One of these pulses correlates in time with the precipitation of mafic trace metals (e.g. Co, Cr, Sc) and the PGEs Pt, Ir, Ru, and Pd from ~94.60 Ma – 94.48 Ma, peaking at ~94.55 Ma. Osmium concentration has its third peak immediately before the peak of these elements at ~94.56 Ma, likely showing a high-resolution indication of when this PGE and trace metal-rich source entered the KWIS. These enrichments have been documented in other locations globally but the timings are not synchronous. In the Comanche Shelf, the time interval of the PGE and trace metal enrichment correlates with a shift to more oxic waters and cooling of global temperature. Some evidence includes bioturbation, a positive $\delta^{18}O$ shift, and the reappearance of northern fauna *Cyclonephelium compactum-C. membraniphorum* into the KWIS via southward migration. The redox behavior of the PGEs in oceanic depositional settings is not well understood, but Cr is well studied. Chromium enrichment in oxic conditions is unusual because it creates mostly soluble species in such conditions. However, Cr^{6+} can precipitate in oxic conditions if replacing Mg in

detrital sediments which is abundant in this interval. Iridium is known to complex with ferromanganese and organic material in oxic conditions, thus seeing a concentration increase in Ir makes sense. The source of these enrichments is most likely volcanic but an extraterrestrial source is also possible. Based on $^{187}Os/^{188}Os$ data, the end of massive LIP input to the oceans occurs at ~94.49 Ma and it takes ~570 Kyr for $\delta^{13}C$ to shift back to pre-excursion values at ~93.92 Ma.

CONTENTS

INTRODUCTION

Ocean anoxic events (OAE) are characterized by global deposition of black shales and ~4‰ positive carbon (C) isotope excursions in organic and carbonate C ($\delta^{13}C_{org}$ and $\delta^{13}C_{carb}$). The isotopic excursion is thought to occur from increased proliferation of primary producers in the oceans and the subsequent burial of their ^{12}C enriched organic matter (Arthur and Sageman, 1994). Supporting evidence is observed in high total organic carbon (TOC; ~3-8 weight %) content in black shales deposited globally. The onset of these anoxic events is associated with increased primary production in surface waters caused by an increase in nutrient supply. This eventually leads to suboxic to euxinic redox conditions (Table 1) in deep waters once the demand for oxygen (e.g., decomposition of organic matter during burial) exceeds the supply in the oceans (Arthur and Sageman, 1994; Monteiro et al., 2012). The first recognition of an OAE in the literature was published by Schlanger and Jenkyns (1976). They recognized coeval deposition of organic-rich black shales in a variety of paleo-bathymetric zones globally during the Cenomanian-Turonian (~93.9 Ma) and Albian-Aptian (~113 Ma) stages, highlighting two distinct OAEs. These events are associated with extraordinarily warm climate, for OAE 2 the likely cause is large igneous province (LIP) eruptions which are exceptionally large bursts of volcanism occuring over a geologically short time period (tens to hundreds of thousands of years). The most prominent and well-studied of all OAE's is the Cenomanian-Turonian OAE 2 (Jenkyns, 2010).

Redox classification of the depositional environments, after Tyson and Pearson (1991)

Redox classes	Oxic	Suboxic	Anoxic	Euxinic
			No free H_2S in the water column	Free H_2S present in the water column
O_2 concentration in bottom waters (ml O_2/l H_2O)	$[O_2]>2$	$2>[O_2]>0.2$	$[O_2]<0.2$	$[O_2]=0$

The values for O_2 concentrations in bottom waters are valid for present-day ocean.

Table 1. Redox classification of depositional environments. Modified from Tribovillard et al., 2006.

The onset of OAE 2 is characterized by submarine LIP (Figure 1) input in the Caribbean and/or High-Arctic (e.g., Snow et al., 2005) fueling enhanced marine productivity by inputting nutrients from the LIP itself (via water/rock exchange and magmatic degassing) and increasing the nutrient input from continental weathering by augmenting storm intensity (Brumsack, 2006; Scopellitti et al., 2006; Turgeon and Brumsack, 2006; Turgeon and Creaser, 2008; Jenkyns, 2010; Monteiro et al., 2012). Osmium (Os) isotopes and concentration data in the Cretaceous western interior seaway (KWIS) elucidate two likely large igneous province (LIP) eruptions. The first began ~50 Kyr before the onset of the $\delta^{13}C_{org}$ excursion (Figure 2) and erupted for ~70 kyr from ~94.94 Ma - ~94.87 Ma (this study). The second erupted for ~ 40 kyr from ~94.74 Ma – 94.70 Ma. These interpretations are based on Os concentration ([Os]) data

paired with a high resolution astronomical calibration (Eldrett et al., 2015) of the Iona-1 that records the entire OAE 2 event with no unconformities.

Submarine volcanogenic eruptions would put an immediate supply of biologically important trace metals (e.g., Fe, Mn, Cr, Co, Cu, Ni, Sc, V) into the oceans via magmatic outgassing and seawater/rock exchange. This in turn increases primary productivity in surface oceans, increasing the amount of life (e.g., phytoplankton, foraminifera) in the oceans, leading to increased oxygen consumption until the demand exceeds the supply in the ocean (Handoh and Lenton, 2003; Monterio et al., 2012; Van Helmond et al., 2014; Holmden et al., 2016). Enrichment in these biologically important trace metals is seen in shallow water carbonates deposited during OAE 2, indicating hydrothermal plumes reached the surface ocean (Eldrett et al., 2014; Orth. et al., 1993). As anoxia spreads, the recycling efficiency of phosphate, an essential macronutrient, increases in ocean surface waters further increasing primary productivity (Tribovillard et al., 2006). In OAE 2s greenhouse climate, the solubility of oxygen from the atmosphere into the oceans would be reduced significantly. Evidence in Li and Ca isotopes (δLi and δCa respectively) has shown the influx of biologically important nutrients from continental weathering is minimal compared to the volcanogenic influx (Pogge von Strandmann et al., 2016; Du Vivier et al., 2015-2).

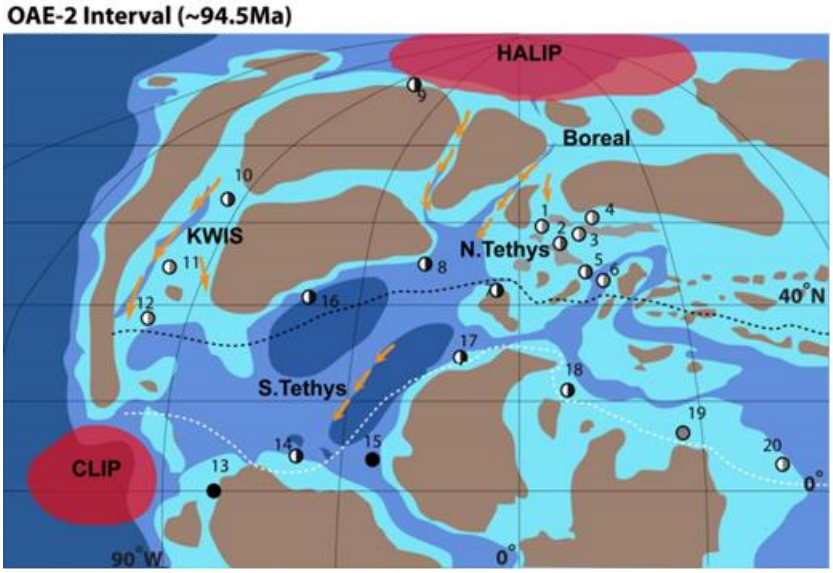

Figure 1. Paleogeographic map showing locations of the KWIS (Cretaceous Western Interior Seaway), CLIP (Caribbean large igneous province), HALIP (High Arctic large igneous province), Iona-1 core (#12), and Portland-1 core (#11) at ~94.5 Ma. Figure modified from Eldrett et al., 2014 who modified after Zheng et al., 2011 and Alexandre et al., 2010.

In this study, the geochemical behavior of PGEs has been examined as there is little data published on their behavior. PGEs are enriched in mantle material relative to the Earth's crust, so during times of prolonged and massive mantle input to the oceans their geochemistry may be of use as geochemical tracers of Earth processes. Indeed, in this study we found the PGEs to be redox sensitive. In oxic conditions, the Pt, Ir, and Ru behave similarly and are enriched in oxic conditions, most likely by complexing with Fe-Mn nodules. Palladium also behaved this way but had anomalous decreases in concentration. In euxinic conditions, all PGEs precipitated in correlation with organic material

GEOLOGIC SETTING AND STRATIGRAPHY

Iona-1 Research Core

The Iona-1 research core was drilled in January 2012 by Shell International Exploration and Production. Its modern-day location is at the confluence of Sycamore Creek and Rio Grande (29°13.51'N, 100°44.49'W) (Eldrett et al., 2015). A $\delta^{13}C_{org}$ chemostratigraphic correlation to the Pueblo Global Boundary Stratotype Section and Point (GSSP) for the Cenomanian-Turonian boundary (CTB) and to the Portland-1 core (Figure 2), another Cretaceous Western Interior Seaway (KWIS) core in a northern paleolocation from Iona-1, has been made (Eldrett et al., 2014). During OAE 2 Iona-1 was in a distal, sediment starved, retroarc foreland basin in the southern gateway of the KWIS (Eldrett et al., 2015). A total of 180 m of core was recovered spanning the lowermost Cenomanian to the lowermost Coniacian (~89-98 Ma) (Eldrett et al., 2014; Eldrett et al., 2016). The upper portion of the Buda Limestone was recovered, followed by the entire overlying 111 m thick Eagle Ford Group (Boquillas Fm), and the lower 40 m of the Austin Chalk (Eldrett et al., 2015). The OAE 2 is represented entirely in the Eagle Ford Group (Gr). It is composed of organic-rich marlstone (marl) beds (avg. thickness ~72 cm), limestone beds (avg. thickness ~ 9 cm) and >300 thinly-bedded, variably reworked, bentonite beds (avg. thickness 4 cm) (Eldrett et al., 2015).

Ages for the Iona-1 were astronomically tuned based on two models by Eldrett et al. (2015) which were also calibrated to Milankovitch cycles recorded in the samples.

The abundance of the most important marine microfossil groups (e.g., calcareous nannofossils, planktic and benthic foraminifers, radiolaria, and dinoflagellate cysts) were calculated which allowed the determination of age diagnostic events. This was paired with geochronometeric (e.g. $^{206}Pb/^{238}U$) dating of zircons from bentonites. The combination of these systems allows for the high resolution dating of the sediments.

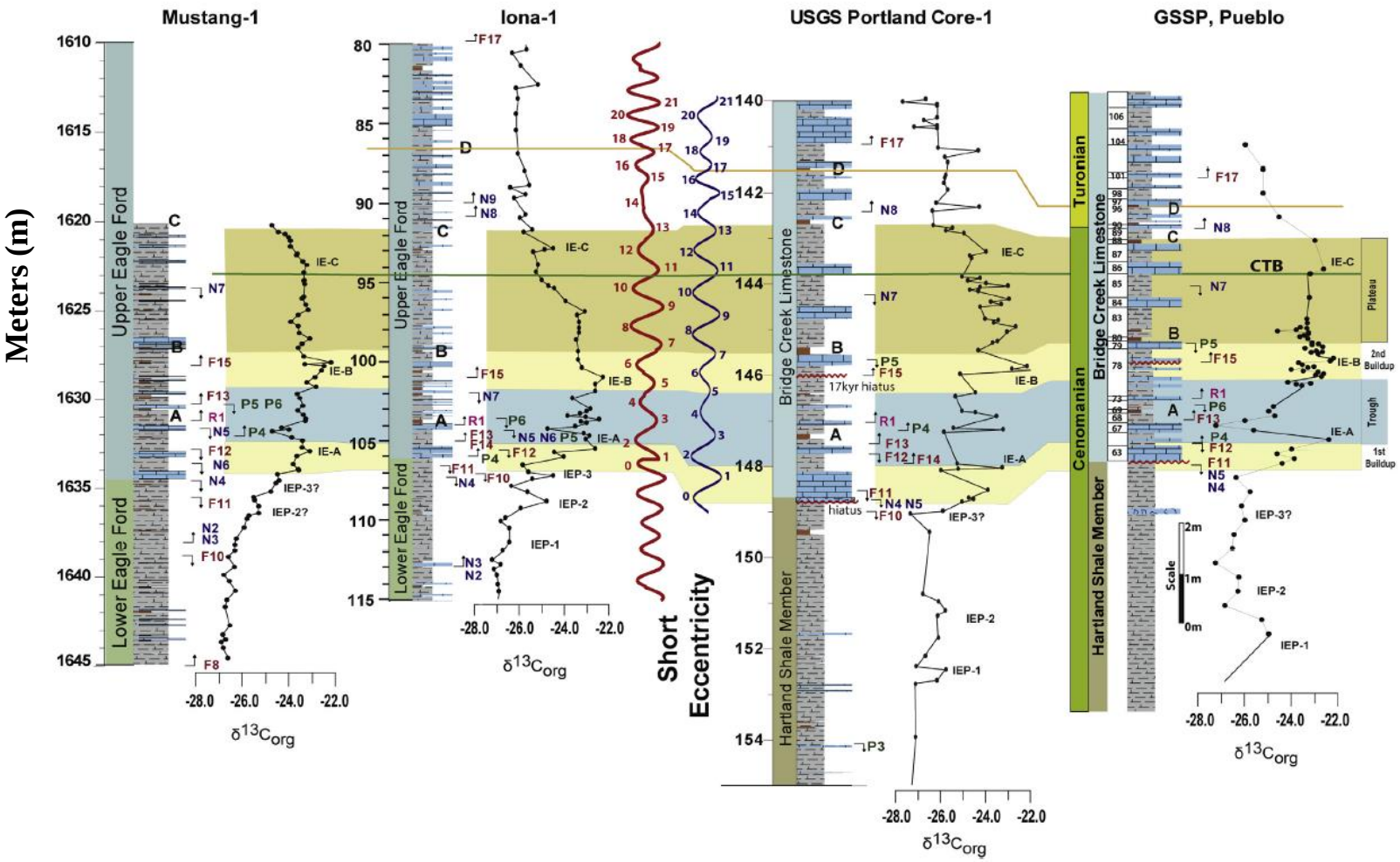

Figure 2. $\delta^{13}C_{org}$ chemostratigraphic correlation of Iona-1 core to USGS Portland Core-1, Mustang-1, and GSSP Pueblo. All depths are in meters. Light brown = bentonites, black = marlstones, blue = limestones, and dark brown = mass transport deposits (MTD). Modified from Eldrett et al., 2015.

Cretaceous Western Interior Seaway and Ocean Circulation

During OAE 2, the KWIS had two connections to the open ocean, one to the north connecting it to Boreal water masses and another to the south connecting it to the proto North Atlantic (Figure 3). Ocean circulation is essential to nutrient delivery and heat transport throughout the ocean and is effected by global climate, thus understanding global temperature shifts and the causes are of importance. Atmospheric CO_2 (pCO_2) levels were significantly higher than today throughout OAE 2, though there is evidence of cooling periods during OAE 2, which has been called the Plenus Cold Event (PCE; Figure 4) (Berner et al., 1983; Jarvis et al., 2011; Jenkyns et al., 2016). To understand Cretaceous ocean circulation, models (e.g., Slingerland et al., 1996; Trabucho-Alexandre et al., 2010), geochemical proxies (Frank, 2002; Zheng et al., 2013) and paleontology (Follimi and Delamette, 1991) have been examined.

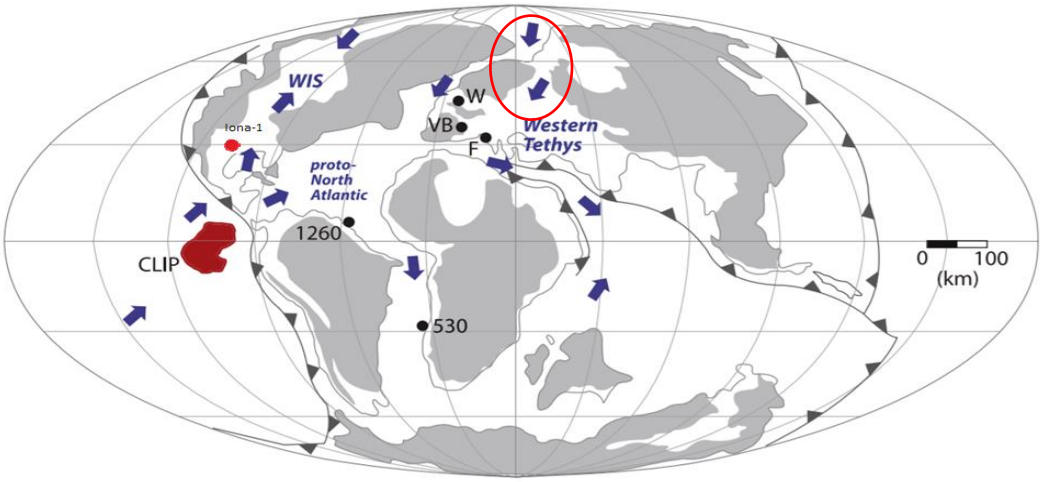

Figure 3. Earth ~93.5 Ma. Paleo-ocean circulation (arrows) and active plate boundaries. Red circle marks the European Shelf Sea. CLIP marks a proposed location for the Caribbean large igneous province. Modified from Du Vivier et al., 2014.

During the latest Cenomanian (~94.7 Ma), there is evidence of abrupt oxygenation of the KWIS seafloor as seen in sudden benthic fauna appearance and geochemical data (Eldrett et al., 2016). This is associated with the PCE and a change in ocean circulation. The cooling event has been proposed to be caused by a slowing/cessation of LIP input into the oceans, which implies a decrease in CO_2 output into the ocean/atmosphere leading to global cooling (Eldrett et al., 2016; Jenkyns et al., 2016). Circulation in the KWIS was modeled by Slingerland et al. (1996) who proposed that continental runoff from eastern drainages exited as a northern coastal jet, and continental runoff from western drainages exited as a southern coastal jet. Outputting of these coastal jets is proposed to have drawn in Boreal and proto North Atlantic water masses creating a strong gyre circulating throughout the KWIS (Slingerland et al., 1996). It is interesting that during a period of global cooling there is evidence of inflowing warm Tethyan water to the KWIS which points towards complex oceanic circulation.

Eagle Ford Group (Gr)

The Eagle Ford Gr represented in the Iona-1 core was deposited below storm wave base (> 100-200 m water depths) in a distal, clastic sediment starved, and restricted setting (Eldrett et al., 2014). It can be divided into an informal upper and lower unit based on differences in characteristics. The lower unit contains abundant finely laminated organic-rich, interbedded marls and limestone with evidence of

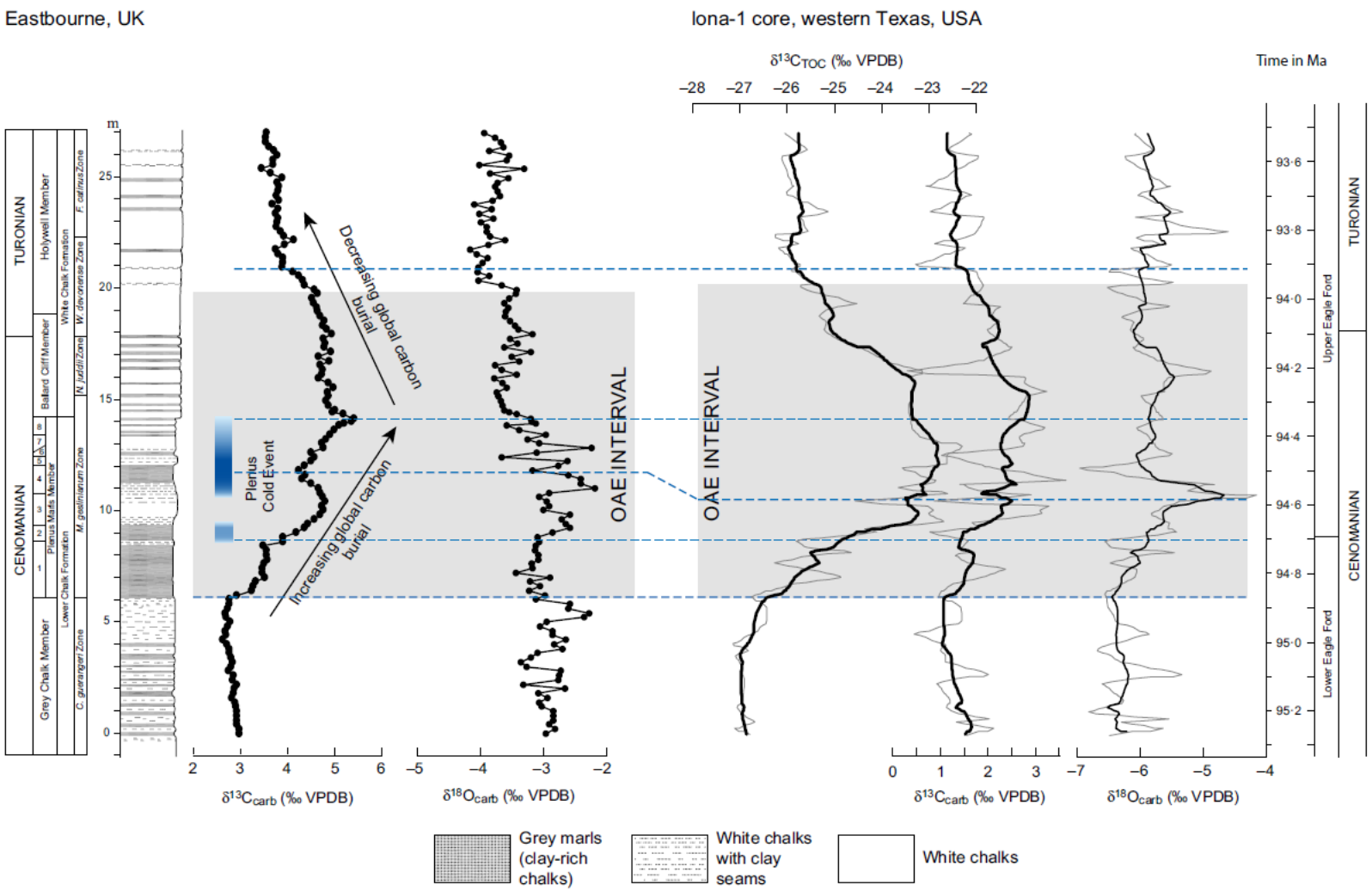

Figure 4. Identification of Plenus cold event on Iona-1 and Eastbourne, UK sections. Modified from Jenkyns et al., 2016.

deposition in a suboxic-euxinic environment with a total organic content (TOC) of ~4-10 wt. % (weight %). The upper unit contains prominent limestone beds, reduced organic content marls with evidence of deposition in a variably suboxic to oxic environment, and relatively low TOC (~0.65-3 wt. %) (Eldrett et al., 2016). The transition from the lower to upper Eagle Ford occurs at ~94.7 Ma (~106.3 m on the core) and is marked by a shift from high to low gamma-ray values attributed to a reduction in organic matter, increase in carbonate content, and fewer bentonites (Donovan et al., 2012; Denne et al., 2014). Ocean anoxic event 2 occurs shortly after the beginning of deposition of the upper Eagle Ford unit, which is seen in the ~4‰ positive $\delta^{13}C_{org}$ excursion (Figure 2). Evidence for the redox conditions at the time of deposition are in trace element concentrations, foraminiferal and nannofossil analysis, and degree of bioturbation of the sediments. Throughout this shift from suboxic-oxic conditions the $\delta^{13}C_{org}$ is unaffected, although, as noted, the TOC wt. % varies significantly.

The Eagle Ford Gr is regionally extensive, spanning ~640 km from the Rio-Grande embayment to the East Texas Basin (Figure 5). Well-log and outcrop correlations indicate that the thickness varies from ~ 12 m to >120 m (Rose, 1972; Donovan and Staerker, 2010). Due to its high TOC and wide geographic extent, the Eagle Ford Gr is one of the largest actively exploited unconventional hydrocarbon reservoirs in the world (Hentz and Ruppel, 2010).

The Eagle Ford Gr studied in the Iona-1 was deposited in the KWIS, an epeiric sea and experienced variations in its connectivity to the open ocean throughout OAE 2. This had a major influence of the redox conditions and nutrient supply in the KWIS, which can explain the differences in redox conditions as compared to the open ocean. In the Del Rio area of the Iona-1, the Eagle Ford is called the Boquillas Fm. In the Texas Gulf Coast the Eagle Ford Gr is known as the Pepper Shale, Cloice Shale, Bouldin Flags and South Bosque Shale (Lowery et al., 2014). The Eagle ford is also equivalent to the San Felipe, Agua Nueva, Cuesta del Cura, and Tamaulipas Fms to the west; the Benton Shale, Indianola Group, Mancos, and Colorado shales to the northwest; and the Tokio and Tuskaloosa Fms to the east (Pessagno, 1969).

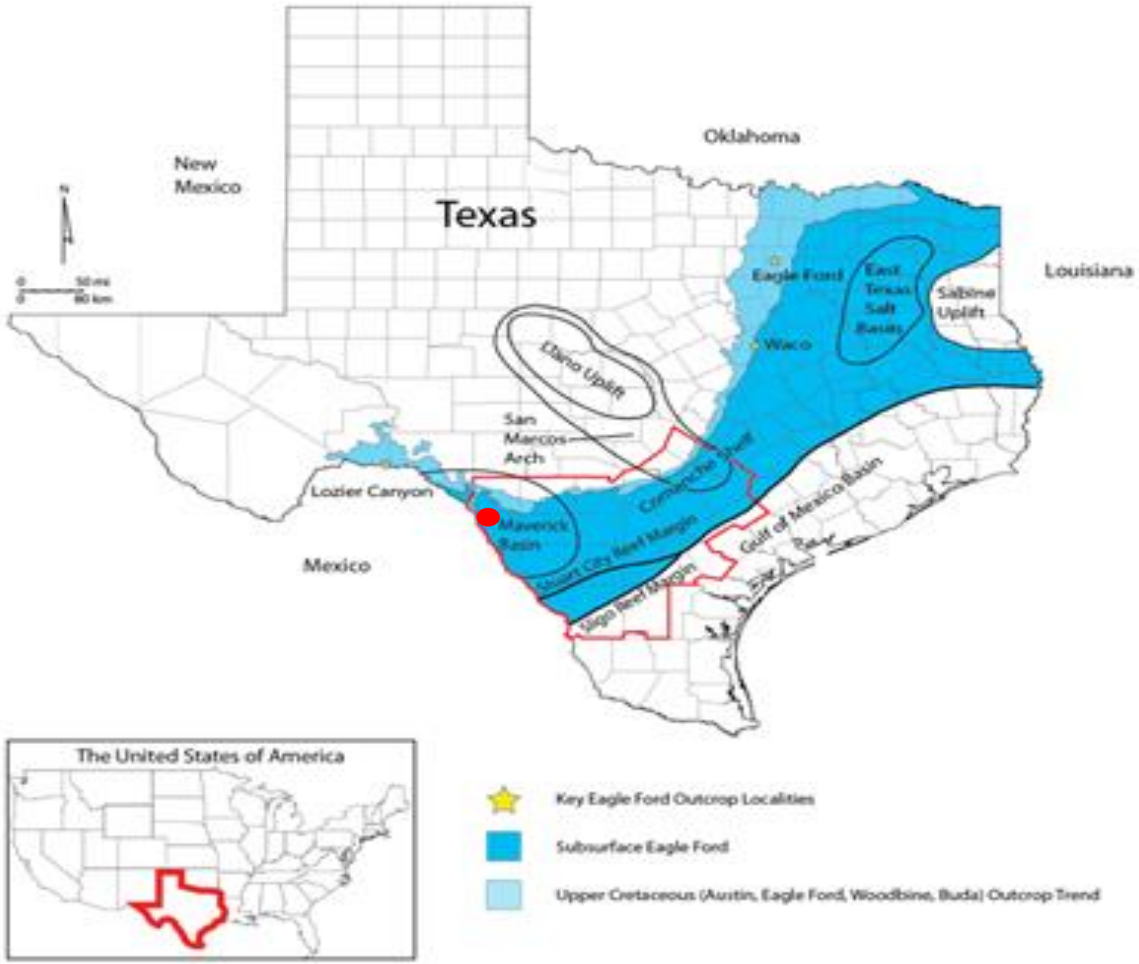

Figure 5. Geographic distribution of Eagle Ford Gr, position of the Maverick Basin, Llano Basin, San Marcos Arch and East Texas Salt Basin in Texas. Iona 1 location marked by red circle. Modified after Harbor, 2011.

Geologic History

In the Early Mesozoic, in a greenhouse climate, the Gulf of Mexico was opened by extensional rifting and sea-floor spreading (Pindell et al., 1988; Salvador, 1991). In the Early Cretaceous, following rift related tectonism, the lithosphere in the northern Gulf Coast region cooled and subsided. This promoted shallow-marine carbonate deposition along low-relief coastal zones during cyclic transgressive flooding and led to the development of a shallow-marine carbonate shelf, known today as the Comanche shelf (Figure 6). (Montgomery et al., 2002; Almon and Cohen, 2008). In the Comanche shelf, during sea level regression carbonate platforms were deposited and during transgression deeper water organic rich (e.g., black shales) facies were deposited (Scott, 1993; Yurewicz et al., 1993). The thickest transgressive deposit in the Comanche shelf is the Eagle Ford Gr. (Montgomery et al., 2002).

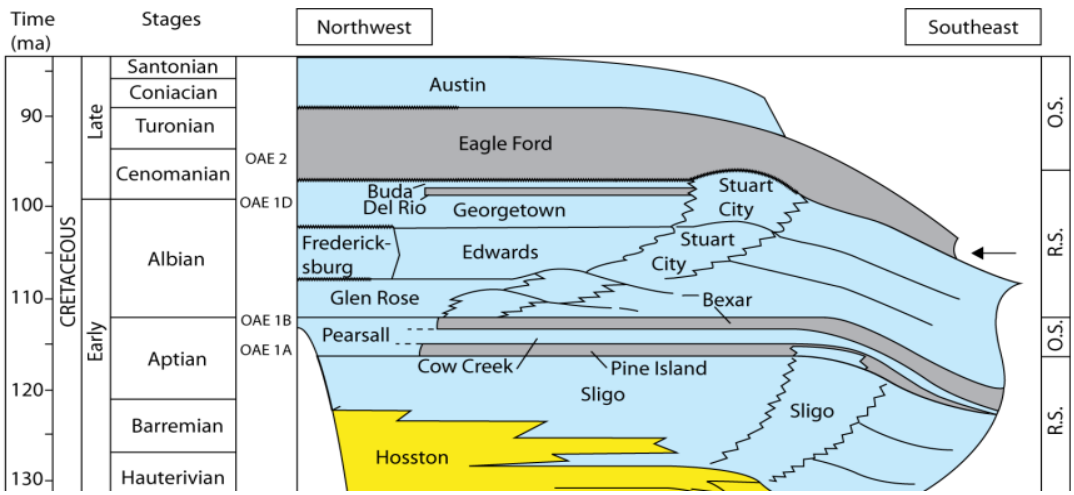

Figure 6. Architecture of the Gulf Coast Comanche Shelf highlighting stratigraphy and age of the EF Group. Modified after Harbor, 2011.

METHODS

Osmium

Osmium (Os) is one of the least abundant elements on the Earth's surface and ocean and is also present in ultra-trace amounts in anthropogenicaly produced metal materials, making any metal used that comes into contact with samples a source of contamination. Hence, the bulk core sample surfaces were thoroughly sanded with carborundum (SiC) to remove any metal contamination from the coring equipment. The bulk rocks (≥30 g) were powdered to homogenize Re and Os (Kendall et al., 2009). Samples were powdered in a Spex rock crusher using a ceramic mixer and ceramic puck that was cleaned in between samples by rinsing with water followed by crushing pure quartz sand and rinsing again. Approximately 0.4 g of powdered aliquots were used in the Os isotope and PGE concentration analyses.

Iona-1 core samples and chemical spikes enriched in ^{99}Ru, ^{105}Pd, ^{185}Re, ^{190}Os, ^{191}Ir, and ^{194} Pt were loaded in Carius tubes with inverse aqua regia; which is 6 ml:3 ml of twice distilled HNO_3 (2xd; starting from Trace Metal Grade) to once distilled HCl (1xd; starting from Trace Metal Grade), respectively. To reduce the Os concentration in the HNO_3, the 2xd HNO_3 was reacted with H_2O_2 following procedures outlined by Yang et al. (2015). Sealed carius tubes were heated in an oven at 220° C for 48 h, equilibrating sample and spikes. Osmium was then selectively purified by solvent extraction with $CHCl_3$ (Cohen and Waters, 1996) then subsequently back extracted into 9 molar (N)

hydrobromic acid (HBr). The residue was microdistilled with a CrO_3-H_2SO_4 solution and collected in 9N HBr following procedures outlined by Birck et al. (1997) and Selby and Creaser (2003). Isolated Os was then loaded onto an ultra-pure (>99.99%) Platinum (Pt) filament and coated with a $Ba(OH)_2$ activator solution for mass spectrometry.

Osmium isotope measurements were made at the University of Houston by isotope dilution negative thermal ionization mass spectrometry (ID-NTIMS) using a Thermofisher Triton Plus following procedures pioneered by Volkening et al. (1991) and Creaser et al. (1991). Osmium was measured as OsO_4^- via ion-counting with a secondary electron multiplier (SEM) detector in peak-hopping mode.

Measured isotopic ratios were corrected for isobaric oxygen interference, instrument mass fractionation ($^{185}Re/^{187}Re$=0.59738 and $^{192}Os/^{188}Os$=3.083), procedural blank contribution, and spike contribution. Analytical uncertainties were obtained by calculating blank abundances, isotopic composition of sample, spike isotopic and abundance values, and the reproducibility of the Os isotopic values of the standard. Average procedural blank was 121.4 ppb. Measurement of an Os standard was the first run for each batch of samples loaded into the TIMS to ensure reliability of the measurements. 500 pg of an Os standard (University of Maryland, Brandon et al., 1999) with a $^{187}Os/^{188}Os$ = 0.11353 ± 0.000376 was loaded onto a platinum filament and covered with a $Ba(OH)_2$ activator solution.

Rhenium and Platinum Group Elements (Re-PGEs)

The residual solutions left after extracting Os with $CHCl_3$ contained Re and the PGEs. The solutions were transferred to a Savillex PTFE beakers and taken to dryness at ~75° C. The dried solutions were then taken up in 0.5 ml of 12N 1xd HCl and subsequently taken back to dryness to convert ions to the chloride species. This was repeated again with 0.5 ml 6 N HCl, taken to dryness, and once again taken up in 0.5 ml 6N HCl and taken to dryness. This process is completed before each new round of column chemistry for anion and cation chromatography. The Re and PGE fractions were purified using anion and cation column chemistry procedures described in Figure 7. All teflon and plastic materials (e.g., pipette tips, centrifuge tubes) were stored in a 1:1 10 N HCl: 1 N HF bath to remove isobaric interfering elements, including Zn, Zr, and Mo on Ru, Pd, and Ir, respectively.

Anion chromatography procedures		
Cleaning	10 ml	MQ
	2 ml	0.8N HNO3
	10 ml	6N HNO3
	10 ml	6N HNO3
	2 ml	0.8N HNO3
	10 ml	10N HCl
	10 ml	10N HCl
	5 ml	1N HCl
	*5 ml	1N HCl
Washing	2 ml	1N HCl
	3 ml	1N HCl
	12 ml	1N HCL + 1M HF MIX
	4 ml	0.8N HNO3
	4 ml	0.8N HNO3
Collecting	12 ml	12N HNO3
	20 ml	12N HCl

Cation chromatography procedures		
Cleaning	5ml	1N HF (ACS)
	1 vol	MQ
	10 ml	6N HCl (cleaning)
	1 vol	MQ
	1 vol	6N HCl (1xd)
	1 vol	MQ
	5 ml	0.15N HCl
Collecting	*1.5 ml	0.15N HCl
	1.5 ml	0.15N HCl
	4 ml	0.15N HCl
	4 ml	0.15N HCl
	TTD @ 120°C	
Washing	1 vol	6N HCl (cleaning)
	1 vol	" "
	1 vol	" "
	1 vol	MQ

Figure 7. Chromatography procedures for Re-PGE samples were converted to chloride species before each round of chemistry. The procedure order is anion, cation, cation. MQ = Milli-Q ultrapure water. TTD = take to dryness.

Anion Columns

Bio-Rad Poly Prep columns were loaded with 2 ml of Eichron 1x8 anion 100-200 mesh resin. The resin was loaded with Milli-Q ultrapure (MQ) water and inspected for bubbles. If any were present, the column was capped and shaken until removed. The resin was then cleaned following anion 'cleaning' procedures (Figure 7). The Re and PGE fractions were dissolved in 5 ml 1 N HCl and loaded into the cleaned anion columns. Anion 'eluting' procedures (Figure 7) were performed and the acid collected from this procedure was disposed of. The Re and PGEs were adsorbed onto the resin while interfering/unwanted anions were washed out. The Re and PGEs were then collected in

teflon beakers following ‘collecting’ anion procedures (Figure 7). The solution was then taken to dryness and prepared for cation columns.

Cation Columns

Bio-Rad poly prep columns were loaded with 1.5 ml of Bio-Rad AG50X-8 100-200 mesh cation resin. The resin was loaded with Milli-Q and inspected for bubbles. If any were present, the column was capped shaken until none were left. The resin was then cleaned following cation ‘cleaning’ procedures in Figure 7. Sample fractions taken from the collected Re and PGE cut drydowns from the anion columns were dissolved in 1.5 ml 0.15 N HCl and loaded into the cleaned columns. Cation ‘collecting’ procedures (Figure 7) were performed and fractions were collected in cleaned teflon beakers. The interfering cations were adsorbed onto the resin while Re-PGEs passed through. The sample was then taken to dryness and the entire cation procedure was run a second time.

In preparation for inductively coupled plasma mass spectrometry (ICP-MS), samples were converted to nitric species, where 30 µl of 2xd HNO_3 was added and samples were taken to dryness. This was repeated twice for a total of three times. Once taken to dryness for the final time, 1.3 ml of 2% HNO_3 was added and the solution was transferred to a 15 ml polyethylene centrifuge tube for mass spectrometry. Throughout conversion and dryness steps, samples were thoroughly inspected for quantitative transfer to make sure nothing was left behind.

The Re and PGE measurements were run on an Agilent 8800 ICP-QQQ (triple quadrupole) at the University of Houston. Standards with Re and PGE were used to correct instrumental mass fractionation. Procedural blanks were 0.9 ppt Ir, 0.2 ppt Ru, 55.0 ppt Pt, 27.5 ppt Pd, and 1.7 ppt Re.

RESULTS

Determination of Initial $^{187}Os/^{188}Os$ Ratios

The $^{187}Os/^{188}Os_{initial}$ of the samples was determined from the equation:

$$(^{187}Os/^{188}Os)_{initial} = (^{187}Os/^{188}Os)_{measured} - (^{187}Re/^{188}Os)_{measured} \times (e^{\lambda t}-1)$$

Where λ is the ^{187}Re decay constant of 1.66×10^{-11} year^{-1} (Smoliar et al., 1996; Selby et al., 2007) and t is the age of the sedimentary rock. A robust chronologic calibration for the Iona-1 has been determined by Eldrett et al. (2016) and individual ages were used for each sample.

Osmium Isotopes and Concentrations

A high resolution initial Os isotope ($^{187}Os/^{188}Os_{initial}$; Os_i) stratigraphy paired with Os concentration data are presented. The Os_i data is in close agreement when compared to Du Vivier et al. (2014) for the KWIS (Figure 8) and the Os_i profile trends are in general agreement with open ocean records (Turgeon and Creaser, 2008; Du Vivier et al., 2015-2). The major difference between the Portland 1 core and the Iona-1, is that Iona-1 records the entire OAE 2 event, whereas Portland 1 one has two unconformities, one at the onset of OAE and another near the middle of the excursion (Eldrett et al., 2014).

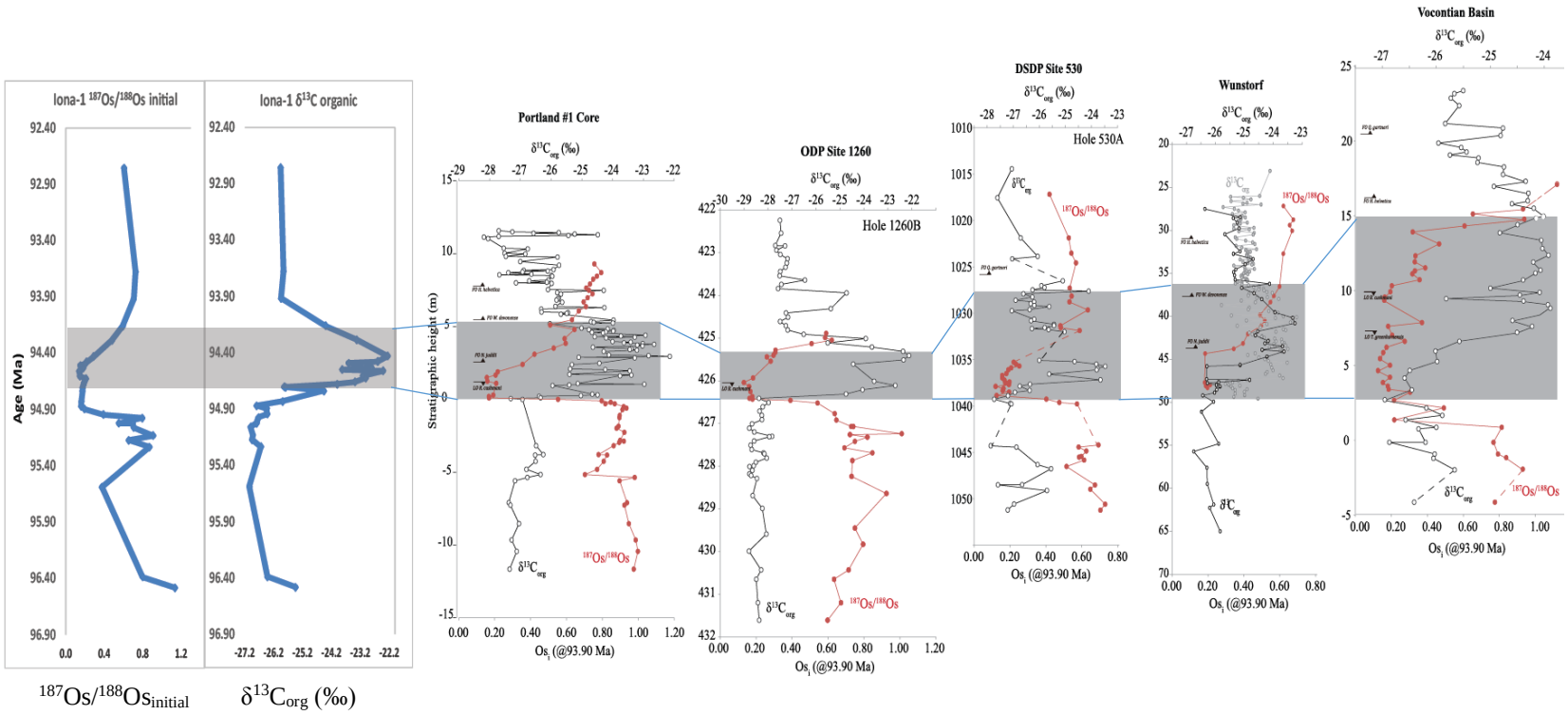

Figure 8. Comparison of $\delta^{13}C$ and $^{187}Os/^{188}Os_{initial}$ data globally. Grey bars represent $\delta^{13}C$ chemostratigraphic correlation between locations. From left to right the name of the sample location and paleolocation are: Iona-1 (KWIS), Portland #1 (KWIS), ODP Site 1260 (S. Tethys), DSDP Site 530 (South Atlantic), Wunstorf (N. Tethys), and Vocontian Basin (N. Atlantic). Modified from Du Vivier et al., 2014.

The present-day residence time of Os in seawater is ~10-50 kyr, most likely closer to 10 kyr than 50 kyr (Oxburgh, 2001; Peucker-Ehrenbrink and Ravizza, 2000; Sharma and Wasserburg, 1997.). This is short enough to record high resolution variations in input fluxes (e.g., continental weathering, hydrothermal, and extraterrestrial) while still being longer than the mixing time of the current oceans (~2 kyr). Thus the oceans are considered to be well mixed and homogenous for Os isotopes. During OAE 2, the residence time was likely much more variable than today due to the increase in Os concentration flux during the event, as well as the variations in output fluxes. The KWIS was an epeiric sea with varying levels of connection to the open ocean (Eldrett et al., 2014; Du Vivier et al., 2014).. At ~96.48 Ma (~1.61 Myr before the onset of OAE 2) the study location is extremely radiogenic (1.2) and Os concentration ([Os]) is extremely low (0.007 ppb) relative to the any other measurement in the core. After this, the Os_i value shifts to intermediate values between mantle and continental weathering of 0.315 to 0.909 and [Os] increases to 0.305 – 0.909 ppb before the onset of OAE 2 (Figure 9). This is evidence of at least some connection to the open ocean as submarine mantle input sources within the KWIS have not been discovered. An alternative explanation is there might have been subaerial volcanic material that was weathered and reached the KWIS. This would all the the unradiogenic shift and [Os] increases to be explained without the KWIS being connected to the open ocean.

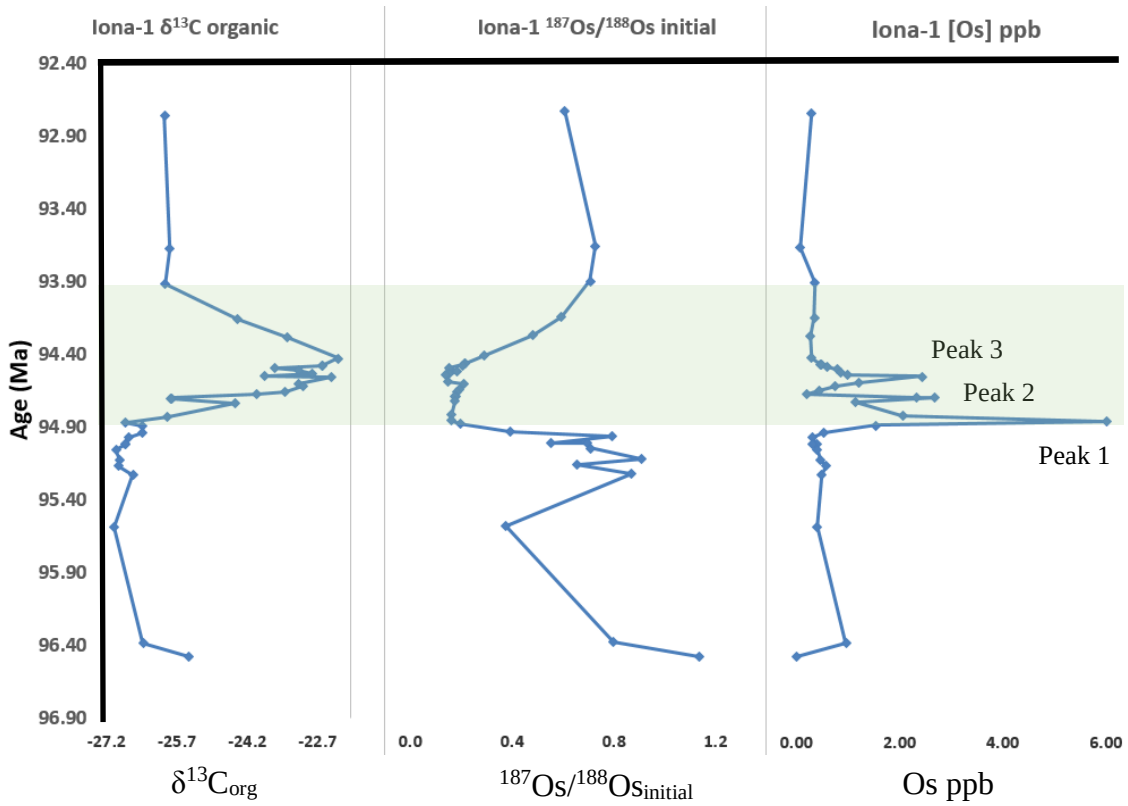

Figure 9. $\delta^{13}C$ organic carbon, $^{187}Os/^{188}Os_{initial}$, and Os concentration in parts per billion (ppb) from Iona-1 samples. OAE 2 is highlighted in blue. Figure shows how the carbon isotope excursion (CIE) was preceded by a shift to unradiogenic 187Os/188Os values paired with an increase in [Os] approximately 50 Kyr before the onset of the CIE. Peaks 1, 2, and 3 indicate highest Os concentrations and are discussed throughout the text. Green bar indicates OAE 2.

Prior to the onset of OAE 2 the Os_i of seawater was radiogenic (0.80 - 1.14) with [Os] averaging 0.484 ppb before the shift to more unradiogenic Os_i values of 0.15 – 0.17 associated with OAE 2. These radiogenic values are likely from continuous continental weathering influx, which has high ^{187}Os and low abundances of any other isotope due to crustal Os mainly coming from the decay of ^{187}Re (Peucker-Ehrenbrink and Ravizza, 2000). In the KWIS the major sources of weathered material came from the Canadian Shield and the Sevier Orogenic Belt (Du Vivier et al., 2014).

Approximately 400 kyr before the onset of the unradiogenic trend, the Os_i of seawater fluctuated between 0.55 and 0.91 (Figure 9) with a relatively stable [Os] ranging from 0.305 – 0.576 ppb. There is no correlation between the more unradiogenic values and higher [Os] and vice versa during this period (Table 2) suggesting the variation is due to fluctuating influences of continental and hydrothermal flux. This likely shows the beginning of increased input of mantle material into the oceans before the onset of LIP activity, and this Os_i pattern is seen in other locations on the Cretaceous Earth (Turgeon and Creaser, 2008; Du Vivier et al., 2014; Du Vivier et al., 2015-2).

Sample	Depth (m)	Age (Ma)	187Os/188Osi	2 SD	Re187/Os188	2 SD	Os (ppb)	2 SD	Ir (ppb)	Pt (ppb)	Ru (ppb)	Pd (ppb)	Re (ppb)	Os/Ir	Pt/Ir	Ru/Ir	Pd/Ir
A	70.45	92.757	0.606	0.021	2511.18	0.68	0.2879	0.0017	0.0158	0.8172	0.0057	0.3826	95.6001	18.17	51.57	0.36	24.15
EFC 1	86.65	93.677	0.727	0.007	418.11	2.42	0.0633	0.0003	0.0157	0.4501	0.0000	0.1838	4.7210	4.02	28.59	0.00	11.68
EFC 20	90.83	93.918	0.707	0.006	898.94	0.74	0.3479	0.0012	0.0055	1.0080	0.0064	0.3785	51.5316	63.78	184.81	1.16	69.40
EFC 21	95.32	94.160	0.593	0.014	583.75	1.43	0.3449	0.0021	0.0075	0.9474	0.0022	0.8929	35.3920	45.92	126.14	0.30	118.88
EFC-2	98.08	94.285	0.481	0.010	630.18	8.19	0.2615	0.0016	0.0164	1.6400	0.0000	0.0000	29.0900	15.96	100.12	0.00	0.00
EFC-3	100.9	94.430	0.291	0.010	541.02	7.03	0.2879	0.0015	0.0082	1.2000	0.0000	0.0000	28.5500	35.24	146.88	0.00	0.00
B	101.83	94.479	0.216	0.002	344.76	0.61	0.4599	0.0010	0.0242	2.7393	0.0212	6.2178	30.3949	18.98	113.03	0.88	256.56
EFC 22	101.83	94.479	0.215	0.002	385.39	0.69	0.4909	0.0011	0.0144	3.5728	0.0682	2.3472	35.9929	34.00	247.42	4.73	162.55
C	102.21	94.493	0.204	0.002	378.75	0.64	0.5930	0.0014	0.0415	3.1980	0.0503	3.3673	42.8418	14.30	77.11	1.21	81.19
EFC 23	102.63	94.510	0.150	0.025	91.42	1.72	0.7811	0.0091	0.0611	5.6023	0.0894	8.6552	14.6045	12.79	91.74	1.46	141.74
EFC 4	102.95	94.532	0.183	0.001	87.56	0.15	0.8671	0.0013	0.0755	3.9571	0.2433	4.8860	15.3660	11.49	52.44	3.22	64.75
D	103.33	94.551	0.151	0.002	113.17	0.41	0.9837	0.0025	0.1748	12.1384	0.5839	0.0000	22.5069	5.63	69.44	3.34	0.00
EFC 24	103.54	94.560	0.140	0.006	67.28	0.94	2.4318	0.0175	0.0986	6.2451	0.2845	6.5439	33.8364	24.66	63.32	2.88	66.35
EFC-25	104.44	94.604	0.149	0.001	83.63	1.09	1.2012	0.0026	0.0901	2.9400	0.0000	0.0000	20.4300	13.33	32.63	0.00	0.00
EFC 5	104.83	94.624	0.211	0.001	110.11	0.34	0.7566	0.0012	0.0249	0.6399	0.0058	0.4163	16.7165	30.43	25.74	0.23	16.75
EFC 26	105.68	94.660	0.191	0.001	61.83	0.31	0.4332	0.0107	0.0098	0.3359	0.0000	0.3552	5.3827	44.14	34.22	0.00	36.19
E	105.95	94.678	0.184	0.003	78.28	1.30	0.1955	0.0006	0.0000	0.2750	0.0000	0.1378	3.0031	0.00	0.00	0.00	0.00
EFC 6	106.45	94.703	0.177	0.001	100.46	0.14	2.3238	0.0037	0.0243	1.2672	0.0373	1.9638	47.1510	95.71	52.20	1.54	80.89
EFC 27	106.5	94.707	0.176	0.001	64.77	0.17	2.6845	0.0056	0.0105	0.9732	0.0054	0.5358	35.3812	256.72	93.07	0.51	51.24
EFC 7	107.17	94.738	0.174	0.001	41.74	0.21	1.1504	0.0017	0.0506	0.8892	0.0239	0.6489	9.8100	22.74	17.58	0.47	12.83
EFC 28	109.22	94.831	0.163	0.001	150.87	0.18	2.0550	0.0034	0.0371	1.0985	0.0336	0.5374	62.1138	55.41	29.62	0.91	14.49
EFC 29	110.01	94.870	0.160	0.000	189.87	2.47	6.018	10.56	0.0260	1.4800	0.0000	0.0000	227.2800	231.71	56.99	0.00	0.00
EFC 9	110.49	94.896	0.195	0.001	223.12	0.25	1.5373	0.0028	0.0136	0.7988	0.0014	0.3938	67.4709	113.00	58.71	0.11	28.95
EFC-10	111.36	94.944	0.412	0.020	1463.74	19.03	0.5186	0.0038	0.0218	1.2000	0.0000	0.0000	117.8300	23.78	55.02	0.00	0.00
F	111.88	94.975	0.794	0.010	1860.27	2.95	0.3148	0.0013	0.0036	0.8544	0.0184	0.6330	82.6074	87.15	236.49	5.09	175.23
EFC 30	112.77	95.023	0.553	0.020	2498.76	5.80	0.3872	0.0022	0.0232	0.8837	0.0153	0.5414	127.7225	16.69	38.09	0.66	23.34
G	112.77	95.023	0.696	0.048	2667.07	13.44	0.3046	0.0027	0.0076	0.9786	0.0000	0.3062	103.7077	39.99	128.48	0.00	40.21
EFC 31	113.42	95.059	0.707	0.013	2398.11	1.68	0.4056	0.0018	0.0000	0.7034	0.0170	0.6852	128.4529	0.00	0.00	0.00	0.00
EFC-11	114.5	95.130	0.909	0.060	2937.31	38.18	0.4733	0.0042	0.0440	1.2400	0.0000	0.0000	169.3000	10.76	28.18	0.00	0.00
H	115.45	95.172	0.654	0.017	2553.13	4.88	0.5759	0.0030	0.0146	1.5845	0.0011	1.0594	185.4018	39.36	108.29	0.07	72.41
EFC 12	116.79	95.234	0.870	0.070	2560.57	33.29	0.4929	0.0049	0.0219	0.9900	0.0000	0.0000	161.6000	22.53	45.25	0.00	0.00
I	124.03	95.589	0.375	0.044	1929.40	9.42	0.3960	0.0037	0.0055	0.8432	0.0109	0.5587	110.6170	71.59	152.44	1.97	101.01
EFC 33	139.86	96.387	0.80	0.013	2737.24	2.78	0.9603	0.0041	0.0169	1.7640	0.0615	1.5931	328.3190	56.65	104.07	3.63	93.99
EFC 34	141.77	96.482	1.14	0.369	2739.96	192.02	0.0072	0.0002	0.0000	0.3168	0.0005	0.0661	2.6805	0.00	0.00	0.00	0.00

Table 2. Concentrations of Os, Ir, Pt, Ru, Pd, Re, 187Os/188Os initial, and 187Re/188Os from Iona-1 core. Values of 0 represent measured concentrations lower than the average blank or no data was collected for the sample. 187Os/188Os$_i$ uncertainties determined by propagation of uncertainties in Re and Os mass spectrometry, spike, blank, and standard Re and Os isotopic values.

After this period, there is an immediate shift to unradiogenic values from Os_i of 0.794 to 0.412 in ~31 kyr paired with an increase in [Os] to 0.52 ppb from 0.31. This is followed by a shift in Os_i from 0.393 - 0.195 paired with an increase in [Os] to 1.54 ppb from 0.52 ppb. This is then followed by a massive increase in [Os] from 1.54 ppb to 6.02 ppb (Figure 9) and a minor shift in the Os_i to 0.160 from 0.195, very close to mantle values. Average upper mantle Os_i is 0.1270 (Widom et al., 1996) and the measured value of 0.160 likely reflects mixing of a dominantly mantle source of Os with minor continental input. This shift to unradiogenic Os_i and elevated [Os] is interpreted to mark the beginning of LIP input and there is evidence in other geochemical tools (e.g., Sr isotopes and mafic trace metal enrichments) to support this. This occurs ~50 kyr before the onset of OAE 2.

The unradiogenic trend (Os_i from 0.140 – 0.211) continues for ~450 kyr but the [Os] varies significantly throughout this time (Figure 9). Some explanations include 1) variations in connection to the open ocean, likely due to local sea-level fluctuations, 2) changes in the input flux of hydrothermal Os to the ocean, 3) large influx of extraterrestrial material causing PGE spikes or, 4) a combination of 1 and 2. The unradiogenic trend occurs immediately before the $\delta^{13}C_{org}$ excursion begins and, in its full ~450 kyr extent, peaks thrice and the [Os] drops sharply immediately after each peak (Figure 9). The three peaks occur at ~94.87 Ma, ~94.71 Ma, and ~94.56 Ma. The first peak is the highest concentration (6.02 ppb) measured and the following two peaks

reach progressively lower concentrations. The second and third peaks will be discussed in the next paragraph.

The onset of the PCE, a period of climactic cooling during OAE 2 with a short warming period in the middle, coincides with the second and third peaks in [Os] and their subsequent decreases (Gale and Christensen, 1996; Jenkyns et al., 2016). Jenkyns et al. (2017) suggested that retardation/cessation of LIP activity could be the driving force behind these cooling periods and the data presented here supports that theory. Our data shows a major decrease in [Os] after the peaks (Figure 9) which can be explained by less/no LIP input to the oceans for a short (~50 kyr) time. If this is the case, the residence time of Os during the Cretaceous would be short (~≤50 kyr) showing a high-resolution recreation of LIP activity. Immediately after the second peak in [Os] (and its immediate decrease) the PCE begins. This is interesting as it implies that the slowing of LIP eruptions coincided with the beginning of the cooling event almost instantly on a geologic timescale. There is a period of warming in the middle of the PCE that coincides with the increase in [Os] leading to the third peak, which could be explained by a continuation of LIP input to the oceans. This third [Os] peak is interesting in that it is near (~9 kyr before) the peak concentration of PGEs (Figure 10) and they correlate with concentration increases in mafic trace metal (e.g., Cr, Co, Sc, Cu, W), all of which occurs during the coldest and most oxic period in the KWIS since the onset of OAE 2.

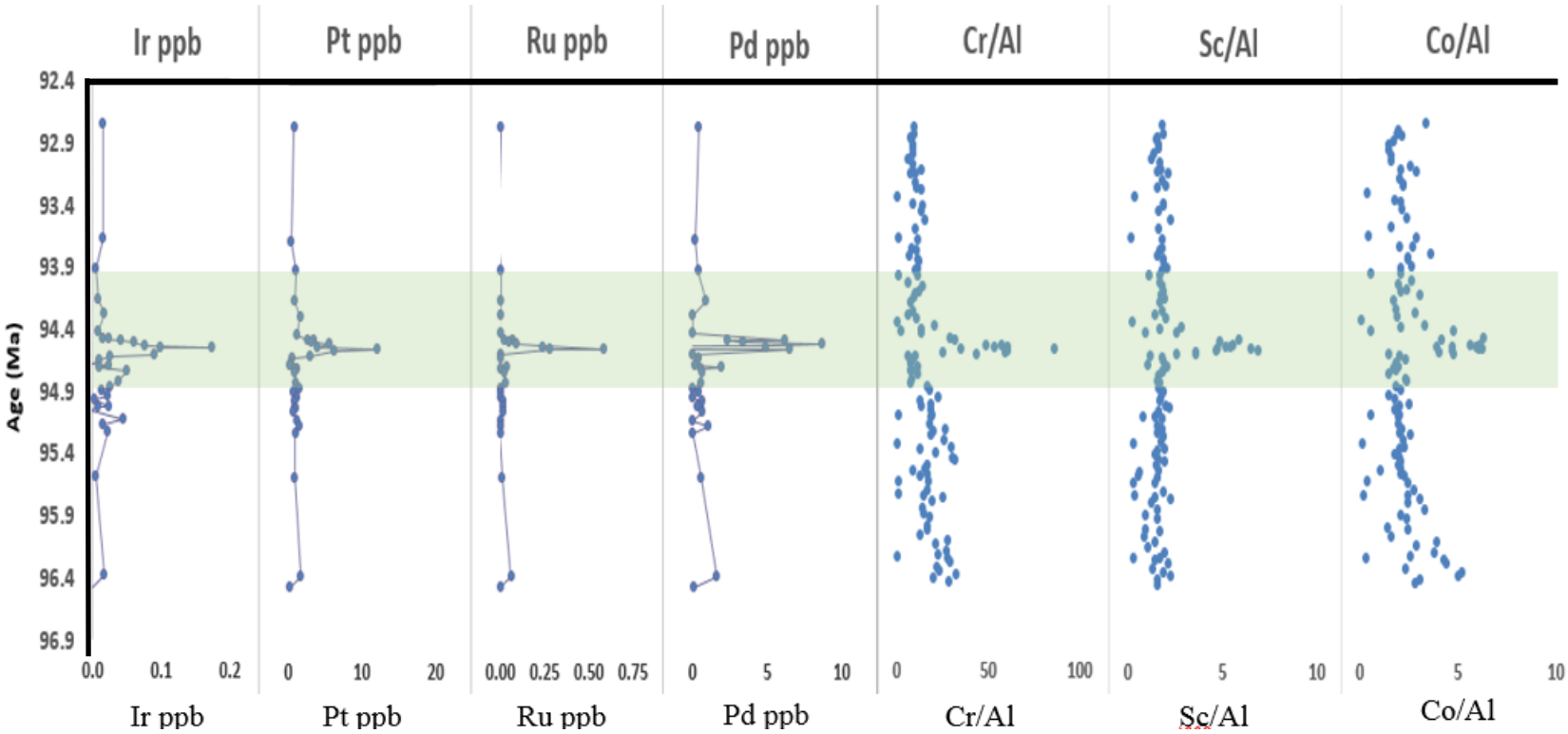

Figure 10. Iona-1 data showing concentration of Ir, Pt, Ru, Pd in ppb and Cr, Sc, and Co are normalized to Al to remove the detrital component from the measurements. Cr, Sc, Co, and Al were measured in ppm prior to normalization. Ru seems to be a narrower peak, but it is important to keep in mind that data from Wright, 2015 was supplemented into this data set and they did not collect Ru or Pd data. The point at the beginning of the excursion correlates to data that Wright, 2015 collected, thus there is just no collected Ru data there. Green bar indicates OAE 2.

The decreases in [Os] after the peaks likely reflects a retardation/cessation of mantle input into seawater and potentially a reduction in circulation with the open ocean. The continuously unradiogenic nature of the Os_i at that time provides good evidence of decreased input of Os to the oceans rather than a circulation disconnection of the KWIS with the open ocean. If, for example, a complete disconnection of the KWIS from the open ocean was the cause of the decrease in [Os], the Os_i would have likely shifted to radiogenic values rapidly, with only continental weathering being the input and having a significant output source available (e.g., TOC wt. % at the peak and immediately after ranges from ~1 - 2.6). There is a very minor shift to slightly more radiogenic values (from ~0.176 to ~2.0; also seen in the Portland 1 (Figure 8) by Du Vivier et al., 2014) between the second and third peaks and this likely reflects an increase in the significance of continental weathering input from a decrease in unradiogenic input and a slight decrease in circulation with the open ocean because this pattern is not seen elsewhere (Du Vivier et al., 2015-2).

After the third peak in the unradiogenic trend, the Os_i increases steadily over time to more radiogenic values (Figure 9) with a nearly homogenous [Os] (0.262 – 0.348 ppb). During this time the $\delta^{13}C_{org}$ is shifting towards more negative values and returns to pre-excursion values at ~94.0 Ma with a Os_i of 0.65.

LIP Sources

There are two proposed zones of LIP input, the Caribbean (CLIP) and the High Arctic (HALIP) (Figure 1). The Caribbean volcanic exposures are more easily accessed than the High Arctic, and thus have been studied more. Both have been dated to have been erupting since before OAE 2 began to long after OAE 2 ended (Tegner et al., 2011; Hoernle et al., 2015). Because LIPS are short, intense volcanic bursts, weathering of the erupted material makes quantifying the surficial extent challenging. The age uncertainties for the CLIP and HALIP are currently large and imprecise. At any rate, a CLIP source was potentially secondary to the HALIP, but because the HALIP is poorly studied due to lack of modern day exposure (Tegner et al., 2011), many have cited CLIP as the source. Indeed, trace metal enrichments seen in the more northern KWIS Portland 1 core ~70 kyr before they are seen in the Iona-1 could be evidence of the HALIP as the source rather than the CLIP. Though this is quite possibly over simplifying ocean circulation patterns. Trace metal analysis of OAE 2 sediments shows a Hawaiian tholeiite composition (Orth et al., 1993). This makes using trace metals to distinguish the HALIP from the CLIP challenging because it seems both were erupting tholeiitic lava with similar chemical signatures at that time (Tegner et al., 2011; Hoernle et al., 2015).

Another challenge in understanding the PGE signal, is understanding how PGEs are transferred from the mantle to seawater. This is currently poorly understood and the modern $^{187}Os/^{188}Os$ of seawater cannot be explained by just hydrothermal alteration

of mantle material. Sharma et al. (2007) collected water samples from Juan de Fuca Ridge, a tectonic Spreading center. Samples came from diffuse and high-temperature hydrothermal fluids, plume fluids, and ridge-flank warm spring fluids as this location type is where Os is thought to be transferred to seawater. Osmium concentration and $^{187}Os/^{188}Os$ were measured and they found that the transfer of Os to seawater via low temperature alteration of mid-ocean ridge basalts (MORB) does not provide enough Os to seawater to account for the $^{187}Os/^{188}Os$ measured in the oceans. Thus, another source of Os to seawater is yet detected. Chen and Sharma (2009) found that surface seawater has a more radiogenic $^{187}Os/^{188}Os$ ratio than deepwaters, which makes other deepwater locations a good place to search for the source. Volcanic outgassing could be a major source of PGEs to seawater, and would be an excellent candidate for study.

Re-PGE Concentrations

There are redox sensitive trace elements (TE; e.g., U, Cu, Ni, Zn, V, Mo) that have been found to be enriched in laminated, organic-rich facies (Figure 11), especially under low-oxygen conditions (Algeo and Maynard, 2004). They exist in multiple valence states that are variably reactive from oxic to euxinic conditions. Of their multiple valence states, the reduced forms are 1) more readily complexed with organic acids, incorporated into solution by authigenic sulfides or precipitated as insoluble oxy-hydroxides, and 2) more strongly effected by precipitating processes in low-oxygen conditions (e.g., increased availability of organic carbon, Mn/Fe redox cycling, and

presence of H_2S at sediment redox boundary or in euxinic seawater) (Pratt and Davis, 1992; Calvert and Pedersen, 1993; Morse and Luther, 1999; Algeo and Maynard, 2004). These processes operate primarily or exclusively in suboxic to euxinic (Table 1) waters. Sediment reworking bioturbators cannot survive in anoxic to euxinic low-oxygen conditions. It should be noted that TEs are not enriched/preserved in bioturbated, organic-poor facies so it is very important that the sediments are undisturbed once deposited (Algeo and Maynard, 2004).

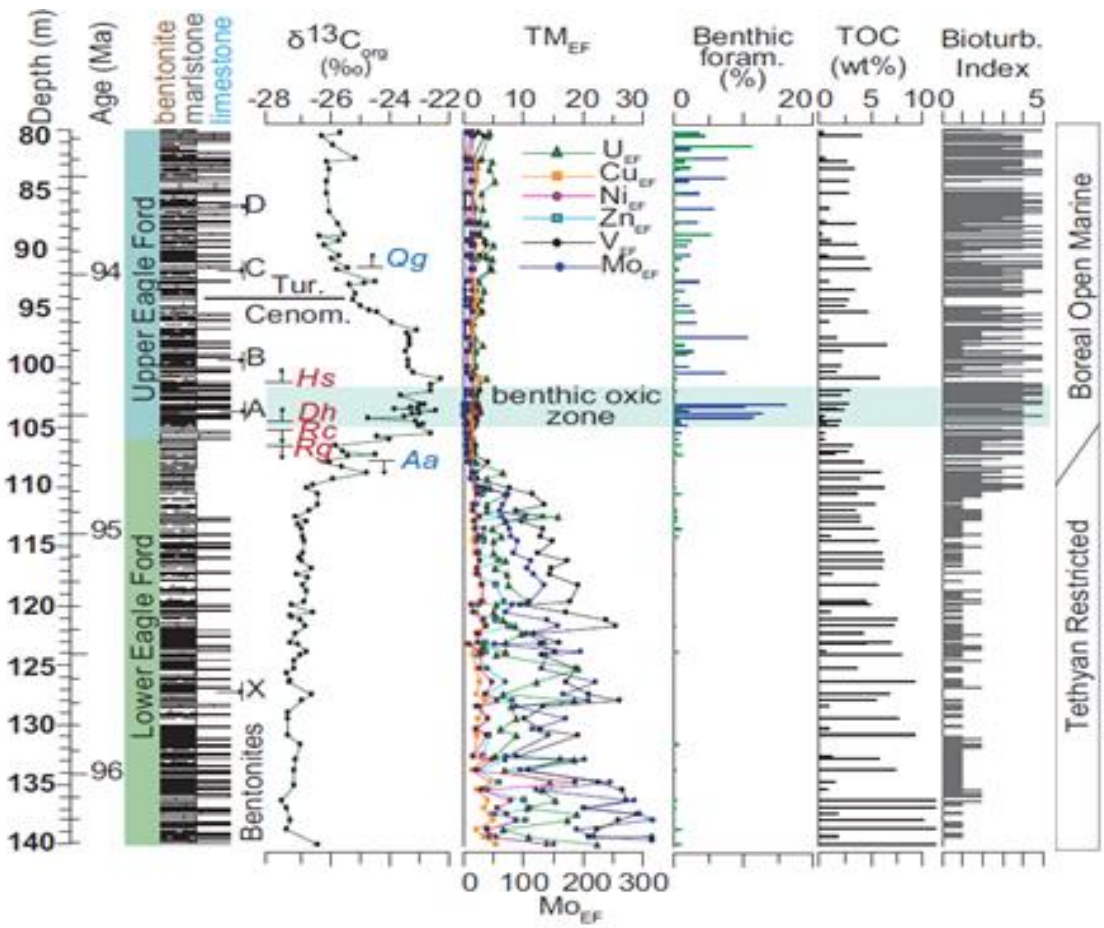

Figure 11. Iona-1 data showing $\delta^{13}C_{org}$, trace metal enrichment factors (TM_{EF}) as proxies for redox condition, benthic foraminifera %, total organic carbon (TOC) weight %, and Bioturbation index (degree of bioturbation. Modified from Eldrett et al., 2014.

DISCUSSION

PGE Overview

The PGE or, *platinum group metals* and *platinoids,* are some of the least abundant elements in the Earth's crust. The PGEs exhibit siderophile and chalcophile behavior (Pachtel, 2016). More than 99% of the PGEs on Earth are most likely in the core because of their incompatibility with silicate melts. PGEs are included in the groups of noble metals (resistant to corrosion and oxidation) and precious metals (rare and naturally occurring with high economic value) due to their inert properties under oxidizing conditions, high fusion temperatures (meaning they are extremely stable in very hot temperatures), and catalytic properties (Puchtel, 2016).

The behavior of PGEs in seawater is just beginning to be understood with the recent development of mass spectrometers with detection limits low enough to measure these elements in their ppb to ppt abundances in crustal rocks. A brief introduction to the behavior of these elements will be discussed based on research available.

PGEs and noble metal speciation stability in seawater is sensitive to redox conditions (e.g., Turner, 2006), seawater pH (e.g., Byrne, 2002), salinity, and temperature (e.g., Au(I) chloride complexes unstable with respect to Au(III) at low temperature but become the dominant species at ~300°C; Gammons, 1996). Iridium, Ru, Pt, and Pd speciation in seawater strongly involve chloride complexation (Byrne,

2002). Of these elements Ir and Ru are minorly influenced by hydrolysis with respect to Pt and Pd (Byrne, 2002). Hydrolyzed Ru (Ru^{3+}) has been found to be strongly pH dependent within the normal pH range of seawater (Byrne, 2002). Current information on the precise aqueous chemical speciation of the PGEs is lacking as far as I have been able to find.

Platinum

The main oxidation states for Pt in seawater are Pt^{2+} and Pt^{4+}, forming the molecules $PtCl_4^{2-}$ and $PtCl_5OH^{2-}$, respectively (Gammons, 1996; Byrne and Yao, 2000). Throughout the normal range of seawater pH, $PtCl_5OH^{2-}$ is the most abundant molecule (Gammons, 1996). One of the major output fluxes for Pt is Iron-Manganese (Fe-Mn) oxyhydroxides in oxic conditions. Covariation between Pt and Mn in the water column shows that in oxic conditions, Pt precipitates with Mn (Jacinto and van den Berg, 1989). Furthermore, Pt has been found to be soluble in the absence of oxygen (e.g., Dymond et al., 1984), data show that Pt can be enriched in anoxic deposits (Goldberg, 1987). It should be highlighted that the anoxic enrichment occurred at a sewer outfall off the coast of Los Angeles, likely indicating an anthropogenic source of Pt that highlights its potential to precipitate from seawater in anoxic conditions. But, the species of platinum may be different that seen in natural conditions.

Palladium

In seawater, the dominant species of inorganic Pd^{2+} is $PdCl_4^{2-}$, with a minor species of $PdCl_3OH^{2-}$ present throughout the normal pH range of modern seawater (Byrne and Yao, 2000). Palladium precipitation from seawater has been found to be correlated with seawater pH (Turner et al. 2006). Palladium reactions, relative to Pt, appear to be rapid and strong which is consistent with a lower particle affinity than Pt (Turner et al. 2006). Palladium has a greater exchange ability than Pt once adsorbed onto sediments, making it more mobile (Turner et al., 2006).

Iridium

A major sink for Ir is Fe-Mn oxyhydroxides in oxic redox conditions (Anbar et al., 1996; Crocker et al., 1973). In low-TOC anoxic settings, Ir has been found to be enriched in seawater and depleted in sediments highlighting its solubility in these settings (Anbar et al., 1996). Our data suggest that Ir may complex with organic material in euxinic conditions, though the fidelity of this correlation needs further testing.

Ruthenium

Ruthenium is the PGE with the least amount of published data available as far as the redox behavior is concerned. Ruthenium has been detected to complex in a range of redox conditions. Enrichments in organic material deposited in euxinic conditions were detected by Lehmann et al. (2007), and it also been found to precipitate in oxic conditions in association with Fe-Mn nodules and phosphates (Bekov et al., 1984).

The concentrations of Os, Ir, Pt, Pd, Ru, Re, and $^{187}Os/^{188}Os_i$, are presented in Table 2. The samples measured have significantly more Os than Ir, and Pt is the most abundant overall with Pd close behind. Mantle sources of Os and Ir have Os/Ir ratios ~≥ 1 (Peucker-Ehrenbrink, 1996, Brügmann and Naldrett, 1988). The samples measured have superchondritic Os/Ir (Figure 12) from 4-256 averaging 33.4. Massive enrichment in Pt, Ir, Pd, and Ru are seen beginning at ~94.66 Ma and ending at ~93.92 Ma. Peak PGE concentrations are Ir: 0.175 ppb, Ru: 0.584 ppb, Pt: 12.138 ppb, Pd: 8.66 ppb, Os: 6.02 ppb, and Re: 328.32 ppb (Figure 13). The maximum enrichment occurs at ~94.55 Ma for every PGE except Pd and Os. The first [Os] peak at ~94.87 Ma does not correlate with an increase with any other Re-PGE except a slight uptick in Re and a slightly delayed (by ~ 4 kyr) increase in Pd.

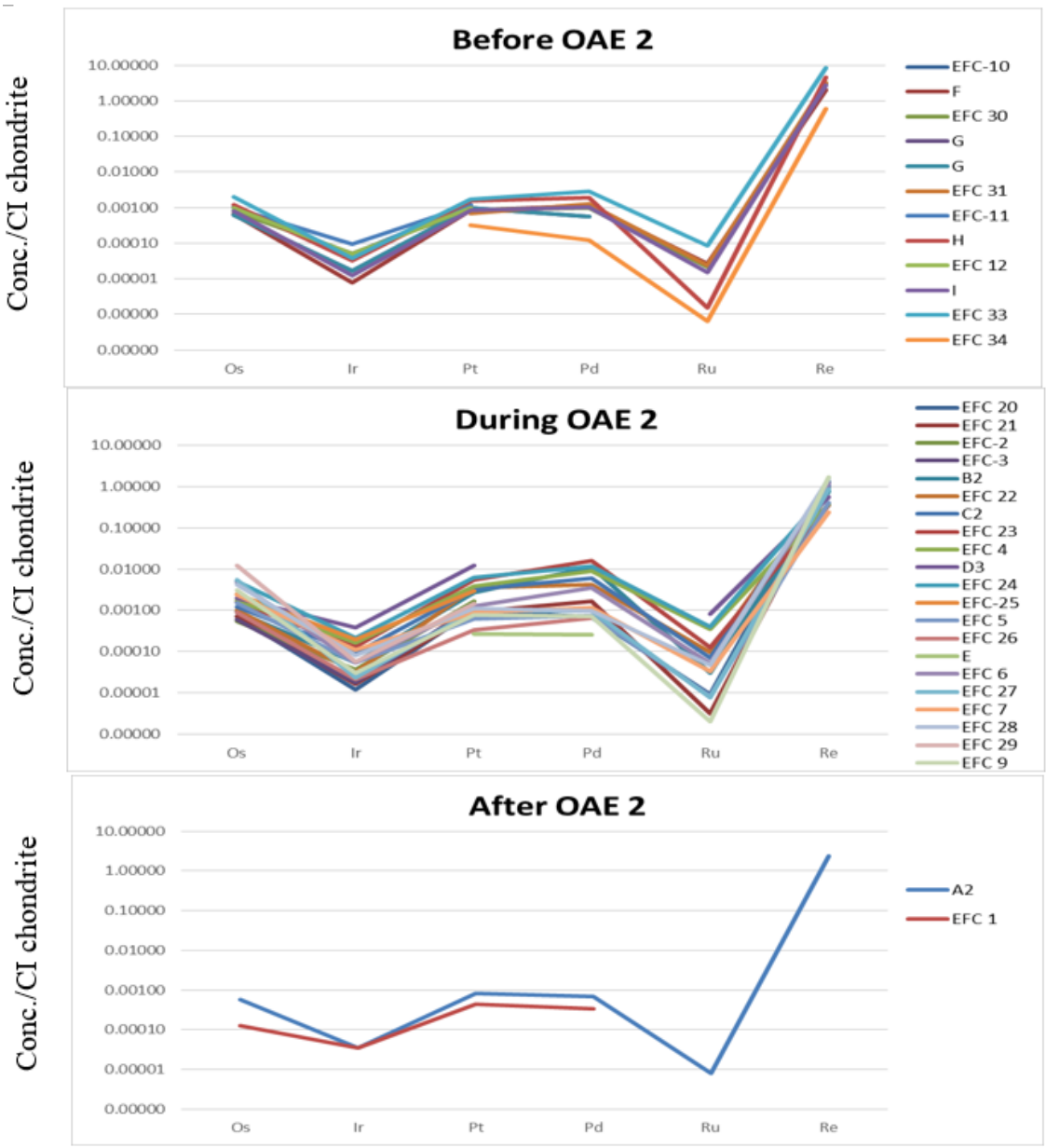

Figure 12. PGE abundances averaged to CI chondrite using values from McDonough and Sun, 1985. Abundance data before normalization for each sample can be found in table 2. Breaks in lines mean no data for that element. Values for chondrite normalization are Os = 490, Ir = 455, Pt = 1010, Pd = 550, Ru = 710, Re = 40 ppb (McDonough and Sun, 1985).

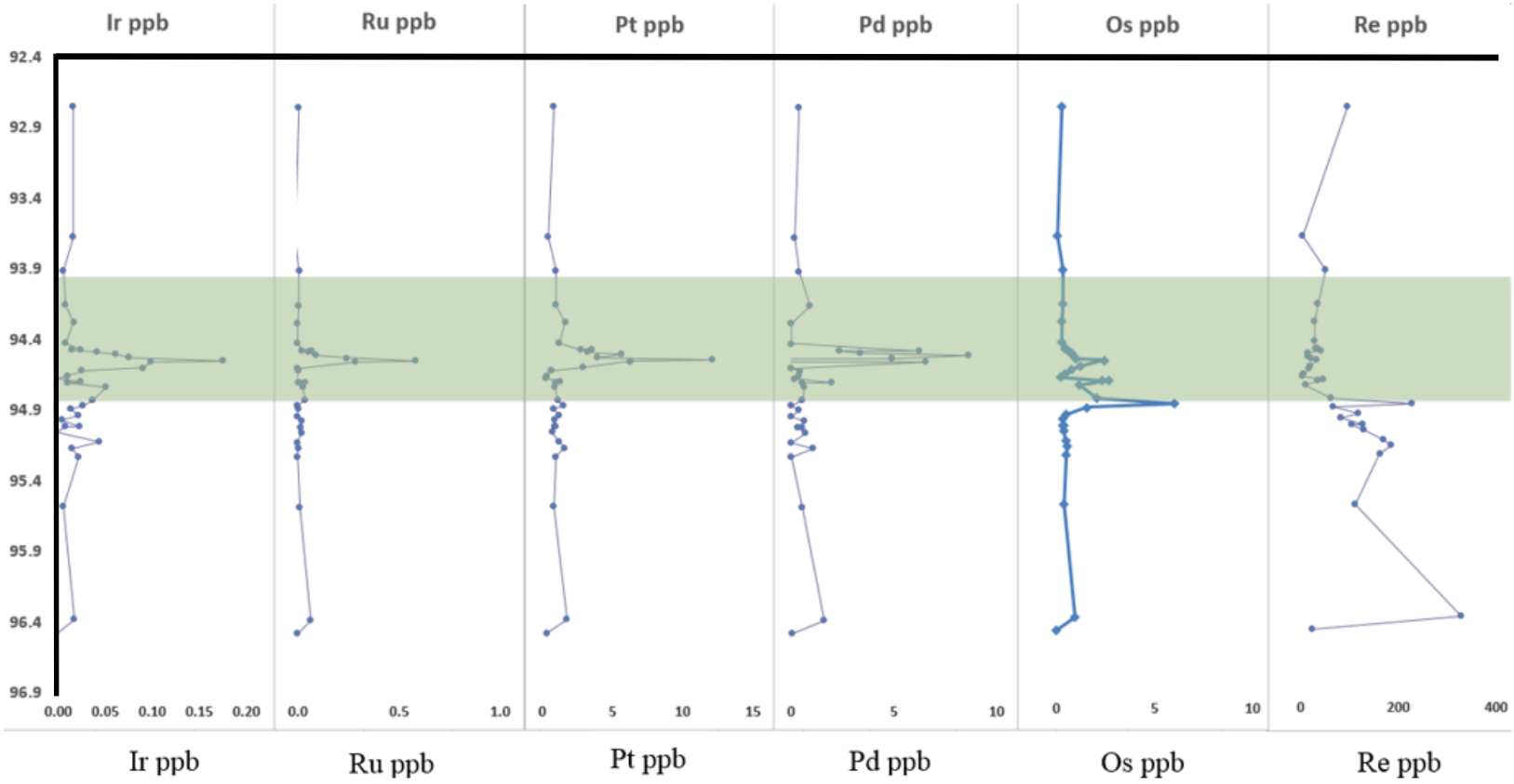

Figure 13. Iona-1 concentrations of Ir, Ru, Pt, Pd, Os, and Re in parts per billion (ppb). Green bar indicates OAE 2.

super chondritic Os/Ir ratios likely occurs from differences in redox behavior between Os and Ir rather than source heterogeneity from an Os/Ir ratio of 1. A major sink of Ir is Iron-Manganese (Fe-Mn) oxyhydroxides in oxic conditions (Anbar et al., 1996) and potentially organic matter under euxinic conditions. Whereas Os is reactive with organic matter and other material (e.g. Fe-Mn oxyhydroxides, sulfides) in any redox condition (Burton et al., 1999; Yamashita et al., 2007). Our data indicate that there is a potential correlation between organic carbon content and Ir concentrations in suboxic – euxinic redox condition.

Reproducibility of Data

Many of the samples tested have been run multiple times. Wright, (2015) ran many of these samples for a thesis chapter. The data collected by Wright, (2015) is compared to the data used in this study (Figure 14; Table 3). Some samples in this study were not run by Wright, (2015) and thus only those data that both ran were compared. Wright, (2015) did not collect Pd or Ru data due to isobaric interference affecting these elements. In this study, updated column chemistry procedures and material (e.g. teflon beakers, pipettes) acid baths were used to remove these interferences. The data collected in this study is in complete agreement with Wright, (2015), with minor variations in the Pt and Ir peaks. This is most likely due to the nugget effect of PGEs. Nevertheless, the overall trends remain the same. Because of the excellent agreement, data from Wright, (2015) that were not run in this study were supplemented into the data set. Of course, these data from Wright, (2015) do not include Ru or Pd. All EFC samples were powdered by Wright, (2015) and aliquots of those powders were used in this study.

Wright, 2015

Sample	Age	187Os/188Osi	[Os] ppb	[Pt] ppb	[Ir] ppb	[Re] ppb
EFC-1	93.7	0.53	0.065	1.460	0.01239	6.03
EFC-20	93.94	0.65	0.340	0.810	0.00780	53.02
EFC-21	94.17	0.49	0.335	1.030	0.00746	39.69
EFC-23	94.57	0.15	0.522	8.760	0.09459	16.52
EFC-4	94.58	0.15	0.805	6.260	0.08333	18.98
EFC-24	94.65	0.14	1.301	5.900	0.17941	39.53
EFC-5	94.68	0.2	0.757	0.640	0.01211	17.75
EFC-26	94.7	0.19	0.418	1.470	0.01118	5.81
EFC-6	94.75	0.16	2.335	1.380	0.01800	51.87
EFC-27	94.755	0.16	2.646	1.230	0.02044	40.07
EFC-7	94.79	0.17	1.138	0.850	0.01259	10.50
EFC-31	95.11	0.79	0.401	0.990	0.01212	126.11

This Study

Sample	Age	187Os/188Osi	[Os] ppb	[Pt] ppb	[Ir] ppb	[Re] ppb
EFC-1	93.7	0.727	0.063	0.450	0.01574	4.72
EFC-20	93.94	0.707	0.348	1.008	0.00545	51.53
EFC-21	94.17	0.593	0.345	0.947	0.00751	35.39
EFC-23	94.57	0.095	0.781	5.602	0.06106	14.60
EFC-4	94.58	0.182	0.867	3.957	0.07545	15.37
EFC-24	94.65	0.046	2.432	6.245	0.09863	33.84
EFC-5	94.68	0.210	0.757	0.640	0.02486	16.72
EFC-26	94.7	0.111	1.486	0.336	0.00982	5.38
EFC-6	94.75	0.177	2.324	1.267	0.02428	47.15
EFC-27	94.755	0.176	2.684	0.973	0.01046	35.38
EFC-7	94.79	0.174	1.150	0.889	0.05058	9.81
EFC-31	95.11	0.705	0.406	0.703	-0.00212	128.45

Table 3. Comparison of Iona-1 samples ran by Wright, 2015 with samples run in this study. Sample, Age (in Ma), $^{187}Os/^{188}Os_{initial}$, Os ppb, Pt ppb, Ir ppb, and Re ppb.

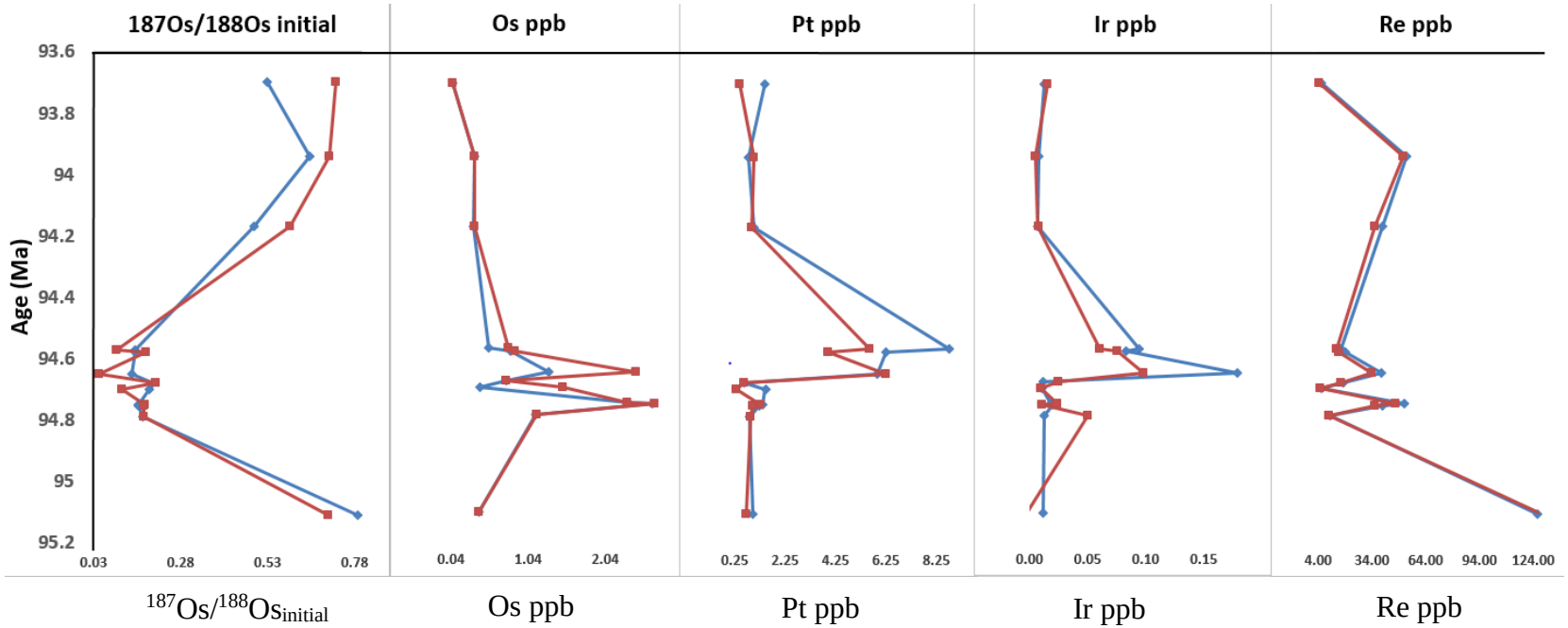

Figure 14. Iona-1 $^{187}Os/^{188}Os_{initial}$, Os ppb, Pt ppb, Ir ppb, and Re ppb data collected by Wright, 2015 (blue) compared to this study (red). Data used to make these graphs comes from table 3.

Outlier Samples

Some samples tested did not produce data from one or more of the Re-PGEs, but never for all of them. Having no data could be due to many reasons including 1) concentrations measured were lower than the blank concentration, so when the data is blank corrected the value comes out less than zero, 2) samples and spike isotopic ratios were too similar and thus a concentration could not be calculated, and/or 3) error in the isolation chemistry. At least some data was collected from all of the samples and errors were uncommon. Samples that are of primary concern are, at the time of this writing, in the process of being rerun and discussed below.

This list of samples will go in order from oldest to youngest (Table 2). EFC 34 did not collect Ir data. Sample I had low counts (~2k CPS on ^{190}Os; which is the spike) for Os when measured on the TIMS and thus the accuracy of ^{187}Os/^{188}Os and [Os] is dubious and is being rerun. Sample G has no Ru data. Sample E has no Ir or Ru data. EFC 26 has no Ru data. Sample D has no Pd data; this one is being rerun as it is the peak concentration for Pt, Ir, and Ru and is in a very interesting location. EFC 1 has no Ru data.

Paleoredox Conditions

Prior to OAE 2, the KWIS water column was anoxic to euxinic and more restricted from the open ocean than during OAE 2 (Eldrett et al., 2014). There is an enrichment in redox sensitive trace metals (e.g., U, Mo, Re, Cu, Zn, V) that are deterministic of anoxic

to euxinic bottom water redox conditions (Figure 11). For example, The U_{EF} :Mo_{EF} (Figure 15) shows a massive enrichment of Mo compared to U at this time. This enrichment occurs from conversion of soluble Mo (which is its stable state in oxic-anoxic conditions) to thiomolybdates that are particle-reactive and rapidly drawn out of seawater in the presence of free H_2S. Molybdenum was likely transported by Fe-Mn oxyhydroxides characteristic of what Algeo and Tribovillard, (2009) describe as a particulate shuttle. Support for this conclusion can be seen in the high TOC content (~4-10 wt%) and low-energy lamination of the organic rich marls deposited during this time.

From the beginning of OAE 2, a gradual depletion of trace metals occured (Figure 11). This could be due to a gradual shift from euxinic/anoxic bottom waters to more oxic seawater conditions. During this time the KWIS's connection to the open ocean was increasing, most likely having a large influence on the shift in redox conditions by introducing open-ocean waters (Eldrett et al., 2014). Evidence for oxic conditions comes from bioturbation of sediments, the appearance of diverse benthic foraminifera (relating to the benthic oxic zone described by Keller and Pardo, 2004), and a decrease in TOC contentment (~0.6–3 wt%). There is a period of mafic trace metal (e.g., Cr, Co, Sc, Mn, Fe, Mg) enrichment that correlates with the PGE enrichment (Figure 10) during this oxic period.

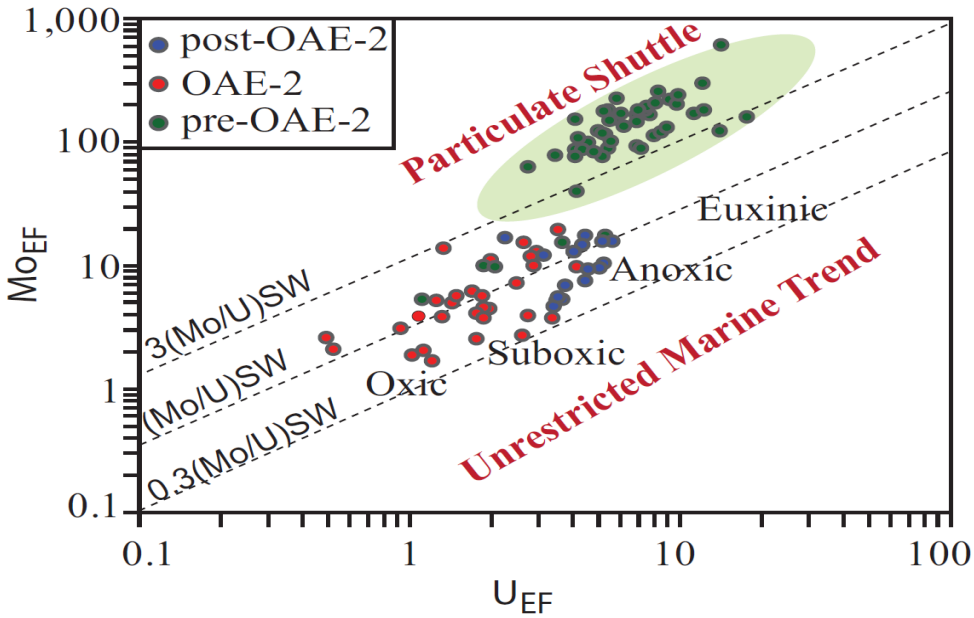

Figure 15. Molybdenum enrichment factor (Mo_{EF}) vs U_{EF}. Enrichment factors are calculated with the equation EF = $(element/Al)_{Sample}$ / $(element/Al)_{average\ shale}$.. Average shale values came from Taylor and Mclennan, 1985. This figure attempts to reconstruct oxic, suboxic and euxinic conditions based on the geochemical behavior of Mo and U. Dashed lines represent different ratios as compared to seawater. Modified from Eldrett et al., 2014

From ~94.66 Ma – ~94.48 Ma, peaking at ~94.55 Ma (Figure 11; Figure 16) an enrichment is mafic trace metals and PGEs is seen. Anomalous increases in these mafic trace metals has been detected by other researchers (e.g., Holmden et al., 2016; Orth et al., 1993; Sinton and Duncan, 1997). Sinton and Duncan, (1997) proposed the enrichments are linked to high-temperature submarine weathering of LIP material during a period of superplume eruptions, though other possibilities such as an extraterrestrial impact can explain this. In the Portland-1 core, a shift to negative $\delta^{53}Cr$ values is detected in the peak [Cr] interval which adds further evidence for a mantle or extraterrestrial source (Holmden et al., 2016). This is discussed in more detail in the Cr isotope section. In Iona-1, this pattern is seen in every PGE except Os which peaks ~7 kyr before the other PGEs.

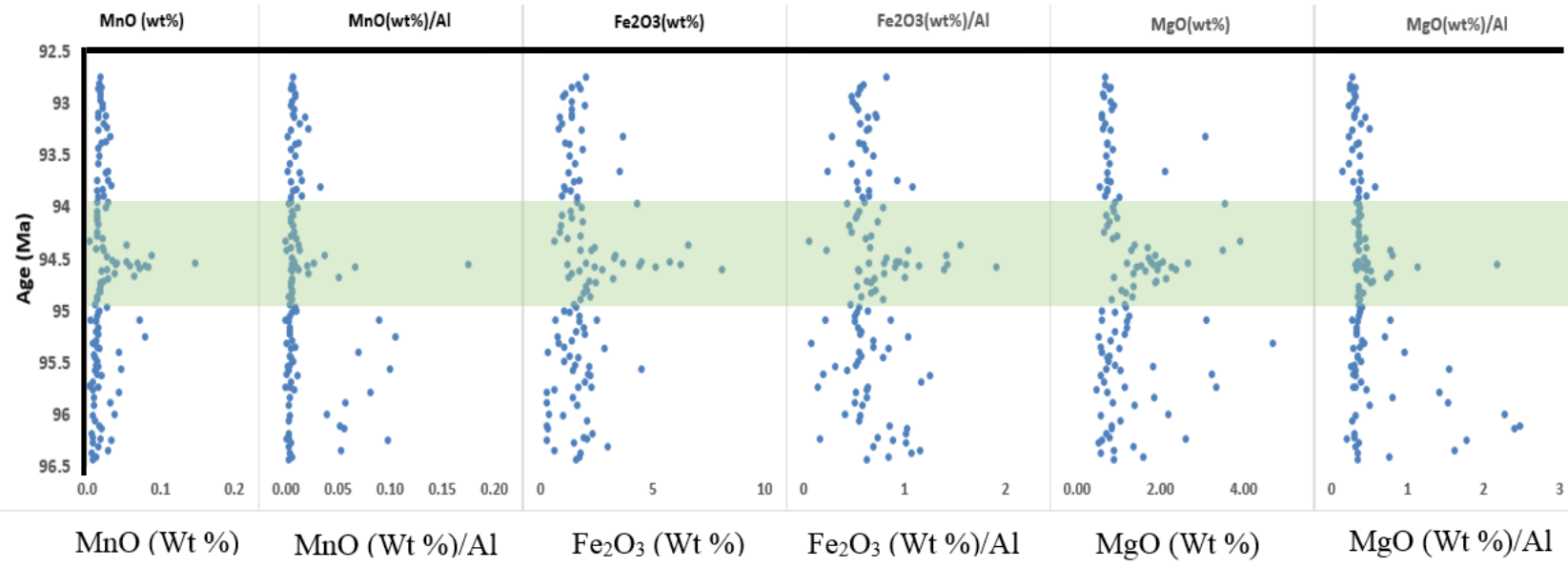

Figure 16. MnO, Fe_2O_3, and MgO weight percent in the Iona-1 core. An enrichment is seen at the interval where the PGEs and mafic trace metals are also enriched. All data also normalized to Al which in theory removes detrital influence on the samples. Green bar indicates OAE 2.

Mafic Trace Element Enrichment

Chromium

Tribivollard et al. (2006) describe Cr and Co as redox proxies with a strong detrital influence. In oxic conditions, Cr is soluble as Cr^{6+}. In anoxic conditions, Cr^{6+} is reduced to Cr^{3+} which forms aquahydroxyl cations and hydroxyl cations ($Cr(OH)_2^+$, $Cr(OH)_3$, $(Cr,Fe)(OH)_3$) that adsorb to Fe-Mn nodules or complex with humic/fluvic acids (Tribovillard et al., 2006). In these forms, Cr precipitates into sediments. Chromium does not form an insoluble sulfide with S (Morse and Luther, 1999), thus it is not precipitated in euxinic conditions and, furthermore, Cr is often removed from organic matter during bacterial sulfate reduction, so Cr would not be enriched in euxinic conditions (Tribovillard et al., 2006). Another way to incorporate Cr into sediments is if it is delivered with land-derived clastic material (e.g., chromite, clay minerals, ferromagnesian minerals where Cr substitutes for Mg; Francois, 1988; Brumsack, 1989; Hild and Brumsack, 1998; Tribovillard et al., 2006).

Cobalt

In oxic environments, Co is found as Co^{3+} or complexed with humic/fluvic acids (Saito et al., 2002; Whitfield, 2002; Achterberg et al., 2003; Tribovillard et al., 2006). In anoxic conditions, Co complexes with S to form insoluble CoS, which can be taken into solid solution by authigenic Fe-sulfides (Huerta-Diaz and Morse, 1992). But, the reaction kinetics of complexing CoS with Fe-sulfides are very slow, so precipitation would lag

behind the creation of CoS molecules. Another way Co will precipitate in oxic conditions is if there is an influx of clastic, detrital material rich in Al, Mn, and Mg (Tribovillard et al., 2006).

It should be noted that at the time of peak enrichment (~94.55 Ma) of the PGEs and mafic trace metals, Al is also at its highest concentration throughout OAE 2 (5 wt. %; average throughout OAE-2 interval is 2.7 wt. %) (Figure 10). Aluminum is often of detrital origin and immobile during diagenesis. At the peak interval the TOC wt. % is 2.5 (Figure 11). This is noted because Cr and Co complex with organic material. During the peak enrichment interval, there is also evidence of bioturbation and the appearance of the boreal (northern) dinocyst fauna *Cyclonephelium compactum-C. Membraniphorum,* which indicate oxic and cool global temperatures relative to the beginning of OAE 2 (Eldrett et al., 2014).

Five sources for the mafic TMs were proposed by Eldrett et al., 2014, 1) basalt hydrothermal alteration, most likely from LIP input, 2) local-scale remobilization within the sediment column (Owens et al., 2012), 3) detrital flux from the Sevier orogenic belt or Canadian shield, 4) Plinian volcanoclastic deposits, which are abundant in the core, and 5) an extraterrestrial impact (Orth et al., 1993). Eldrett et al. (2014) favored LIP emplacement and submarine weathering, citing that the coincident enrichment in Fe did not support evidence of a detrital source. The TM anomaly is seen in the Portland-1 core ~70 kyr before it appears in the Iona-1. This could mean that there was a boreal

source of these trace metals, possibly from alteration of HALIP material. An influx of northern waters could be supported by Zheng et al. (2013) who found a negative εNd excursion in the NW European shelf sea (Figure 4) and attribute it to an influx of boreal waters. To extend the inflow to the KWIS, which was experiencing a sea level maximum, does not seem like a stretch.

Another KWIS core, Portland-1, also has [Cr] and [Co] increases but they occur at different times (Figure 17), with Co peaking before Cr. In Portland-1, Cr has its peak when Os_i is beginning to shift to radiogenic values of 0.3-0.5 which indicates a cessation of LIP input to the oceans and a return to radiogenic seawater values (which correlates at ~94.49 Ma in the Iona-1). The decoupling of these elements is interesting because the Iona-1 shows consistency between not only these trace elements, but also Pt, Ir, Ru, Mg, Mn, and Fe. An explanation for the decoupling of Co and Cr in the Portland-1 is currently unavailable.

An argument could be made in support of an extraterrestrial impact. A hypothetical extraterrestrial impact in the northern hemisphere could also explain the TM and PGE increased flux and why the enrichments correlate to a cool rather than warm period. This impact would most likely be subaerial to explain the increased Al components seen in the sediments as well as why a Cr enrichment is seen under oxic conditions. Orth et al. (1993) detected Ir anomalies globally that correlate with this time. The KWIS sediments have the greatest enrichment, and an extremely weak but

present Ir peak in modern European sediments. If the HALIP was the source of the element anomalies it could be argued that the European shelf should have equal proportions of the anomaly. To solve this conundrum redox conditions could be determined to see if they are conducive to drawing down these trace elements; meaning potentially different redox conditions at each location where these trace metals would precipitate.

Fe-Mn-Mg Enrichment

Along with the trace metals and PGEs, Fe, Mn, and Mg also follow the same pattern and peak at the same location (Figure 16). Iridium is known to precipitate by complexing with Fe-Mn oxyhydroxides in oxic conditions which can explain its enrichment. Manganese-oxide minerals can oxidize insoluble Cr^{3+} to soluble Cr^{6+} (Eary and Rai, 1987). Thus, to have Cr precipitate not only in oxic conditions, but when there is also the increased presence of MnO to convert Cr^{3+} atoms in seawater to Cr^{6+} is paradoxical. Potentially a detrital influx to the Maverick basin during OAE 2 could explain how Cr is precipitating in oxic conditions. Chromium can replace Mg in detrital sediments which could allow it to precipitate in an oxic environment (Tribovillard et al., 2006).

Cr Isotopes

Chromium is a stable isotope tracer where mass dependent fractionation occurs when Cr^{6+} is reduced to Cr^{3+} (Ellis et al., 2002). Lighter Cr isotopes are preferentially reduced from Cr^{6+} to Cr^{3+} by reducing agents (e.g., Mn-oxide, magnetite, sediments) (Ellis et al., 2002). The fractionation factor for this reaction varies between -0.4‰ and -5.0‰ (Ellis et al., 2002; Sikora et al., 2008; Scheiderich et al., 2015).

In the KWIS Portland 1 core, Holmden et al. (2016) measured $\delta^{53}Cr$ and [Cr] (Figure 17) and detected a negative shift in the $\delta^{53}Cr$ ratio of ~0.7 to approximately mantle values (0.124) that occurs with the increase in [Cr] from ~1 ppm to ~28 ppm.

Holmden et al. (2016) created a mixing model and calculated that ~90% of the Cr in the peak interval came from a mantle-like source. A mantle source of Cr would input Cr^{3+} to seawater and would be associated with anoxic waters (Holmden et al., 2016).

If the Cr anomaly came from LIP input to the oceans, why does the Os_i and [Os] shift occur before shifts in Cr geochemistry? Holmden et al. (2016) proposed that the input of Cr^{3+} could have been oxidized to Cr^{6+} and thus was soluble in seawater until a later event that reduced and precipitated the Cr.

Chromium Geochemistry – Portland #1

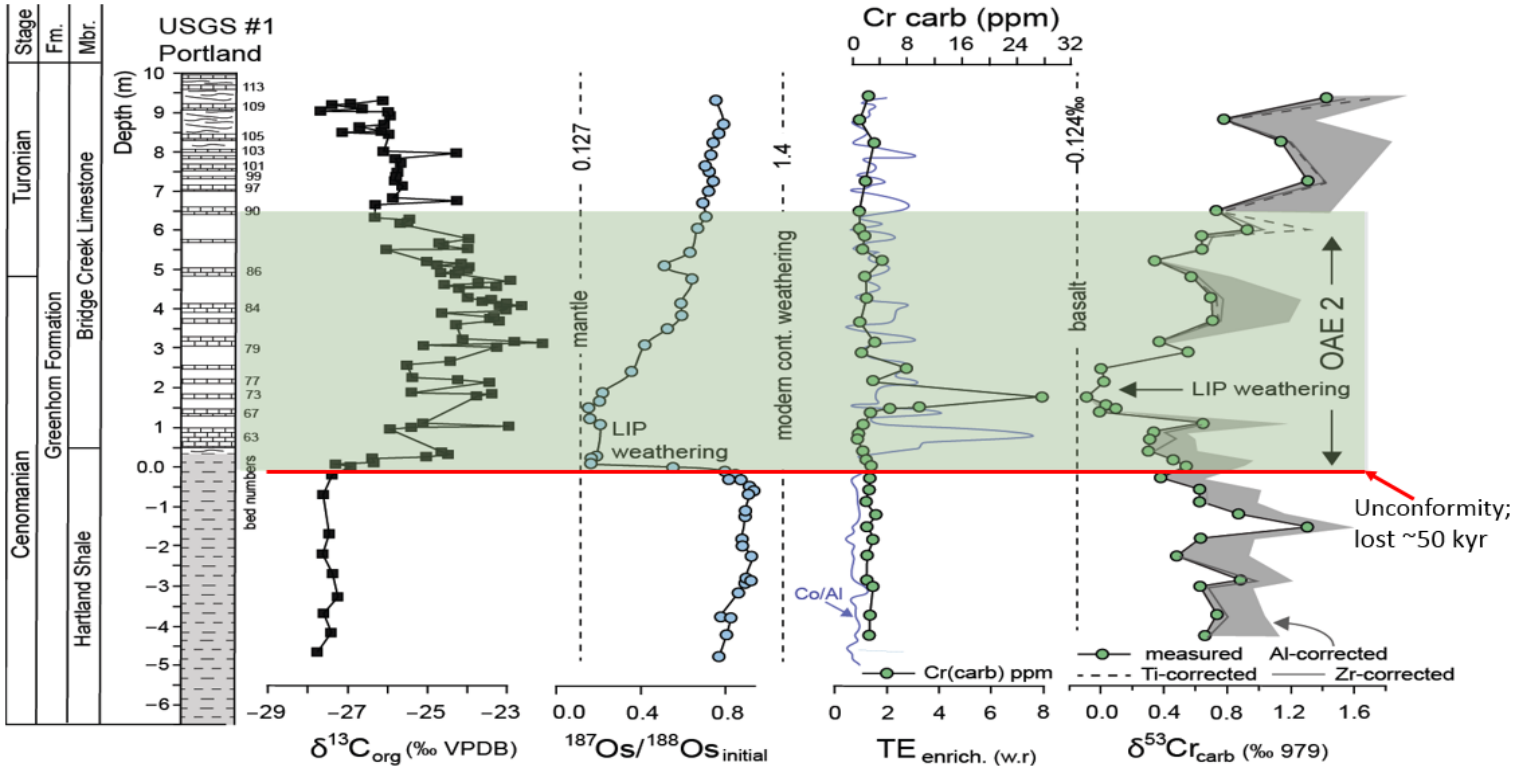

Figure 17. Portland-1 δ13C, 187Os/188Os, Cr, Co, Cu enrichment factors, and δ^{53}Cr data. Trace element enrichments calculated with equation: $TE_{element/Al}$ = (element/Al)measured/(element/Al)average shale (Brumsack, 2006). Red line highlights unconformity at the onset of OAE 2. Green bar represents OAE 2. Modified from Holmden et al., 2016.

CONCLUSION

The behavior of Os and the other PGEs is decoupled throughout OAE 2 in the Eagle Ford Gr prior to and throughout OAE 2. Os geochemical behavior follows its own pattern that is not reproduced by any other measured element. Three major peaks (Figure 9) in [Os] were detected that correlate with warming periods when [Os] is increasing immediately followed by cooling periods after these peaks, known in publications as the PCE. This is interpreted as timing of submarine LIP eruptions that initially lead to the onset of OAE 2 after the first peak, and the extensions of OAE 2 via the next two peaks.

Measured $^{187}Os/^{188}Os_{initial}$ values reveal that massive unradiogenic material was input to the oceans and precedes the CIE by ~50 kyr. This suggests that the residence time of Os in seawater is similar to today (~10-50 kyr) and that the [Os] record shows three major inputs of unradiogenic material into the oceans. The location of the LIP eruption is still uncertain. Many publications cite the CLIP as the source, but dates of CLIP material are uncertain and further work is needed to prove this.

The enrichment of Ir, Pt, Ru, and Pd occur with the mafic trace metals Cr, Co, Sc, Mn, Mg, and Fe. The enrichment of these elements occur when the KWIS is fully connected to the open ocean and there is evidence of oxic and cold conditions via bioturbation and the reappearance of the boreal fauna *Cyclonephelium compactum-C. membraniphorum*. Thus, the precipitation of the PGEs is likely due to seawater

conditions becoming oxic, which allowed them to leave seawater as a new insoluble species. The enrichment of the trace metals is also seen in the northern KWIS Portland-1 core and occur ~70 kyr before they appear in the Iona-1 core. This could mean that the source of these elements comes from a boreal location rather than from the CLIP eruption as the Portland-1 would have been geographically closer.

The maximum concentration measured of the Re-PGEs are: Os = 6.02 ± .011 ppb, Ir = 0.175 ppb, Pt = 12.14 ppb, Ru = 0.584 ppb, Pd = 8.66 ppb and Re=328.32 ppb. The max concentrations of Pt, Ir, and Ru occur at ~94.55 Ma, Os occurs at ~94.87 Ma, and Pd occurs at ~94.51 Ma. Palladium has anomalous decreases in concentration during the peak interval that are decoupled from the other PGEs. This is likely due to analytical errors, most likely because the sample and spike isotopic ratio were too similar and thus a concentration could not be calculated. Very high counts per second (CPS) were measured for this sample (sample D).

Cr geochemical behavior is well studied. Cr is generally soluble under oxic conditions. Thus, to see an enrichment of Cr during the most oxic interval is surprising. Cr is known to replace Mg in detrital sediments in oxic conditions (Tribovillard et al., 2006) and we see an enrichment in MgO wt%. (Figure 16) during this peak interval. Another oxic output of Cr is carbonates (Hua, et al., 2007; Tang et al., 2007), were also present during the enrichment period. The replacement of Cr for Mg is most likely how we see the enrichment of Cr in oxic conditions. The next question to answer is, what is

the source of the Mn, Mg, Fe, Cr, Co, and PGE? Two likely explanations are 1) A mantle source or 2) an extraterrestrial source. Many researchers have cited a mantle source for these enrichments but it is interesting that there was LIP input for hundreds of thousands of years before this and these enrichments are not seen in those intervals. It could be due to the redox conditions making them soluble in seawater. These elements could have been soluble and in euxinic to suboxic seawater since the beginning of LIP input, and finally precipitated when the bottom waters became oxic. A counter argument could be made if the third peak in [Os] at ~94.56 Ma corresponds to a new input of unradiogenic material to the ocean. In this case, the input of this material occurs immediately before these elements are enriched at ~94.55 Ma, and the source of this material was also enriched in Mg, Fe, and Mn allowing Cr to precipitate in oxic conditions.

Future work needs to be done on the transfer of PGEs from the mantle to seawater as it is currently poorly understood. For example, the modern-day transfer of Os to seawater via low-temperature alteration of mid-ocean ridge basalts (MORB) does not provide enough Os to seawater to account for the $^{187}Os/^{188}Os$ measured in the oceans (Sharma et al., 2007). Thus, another source of Os to seawater is yet detected. This has major implications during OAE 2 for all Re-PGEs. A potential mantle source could be high-temperature outgassing, which would have been much more abundant during OAE 2 than today. Nevertheless, more work needs to be done to constrain 1) how Re-PGEs are transferred to seawater, 2) How long it takes for mantle material to be

reacted into seawater, 3) The redox behavior of Re-PGEs, and 4) high-resolution recreation of global temperatures and pCO_2 before, during, and throughout OAE 2 to know how long it took Earth to recover to pre-OAE 2 conditions.

REFERENCES

Achterberg, E., Van den Berg, C., and Colombo, C. 2003. High resolution monitoring of dissolved Cu and Co in coastal surface waters of the western North Sea. *Contin. Shelf. Res.* Vol 23. 611-623.

Algeo, T. and Maynard, J. 2004. Trace-element behavior and redox facies in core shales of Upper Pennsylvanian Kansas-type cyclothems. *Chem. Geo.* Vol 206. 289-318.

Algeo, T. and Tribovillard, N. 2009. Environmental analysis of paleoceanographic systems based on molybdenum-uranium covariation. *Chem. Geo.* Vol 268. 211-225.

Almon W. and Cohen P. 2008. Palaeoecological significance of turritelline gastropod-dominated assemblages from the mid-Cretaceous (Albian-Cenomanian) of Texas and Oklahoma, USA. *Cretaceous Research.* Vol 29. 65-77.

Anbar, A., Creaser, R., Papanastassiou, D., and Wasserburg, G. 1992. Rhenium in seawater: Confirmation of generally conservative behavior. *Geochem. et Cosmochem. Acta.* Vol 56. 4099-4103.

Anbar, A., Wasserburg, G., Papanastassiou, D., and Anderson, P. 1996. Iridium in natural waters. *Science* Vol 273. 1524-1534.

Barbante, C., Veysseyrw, A., Ferrari, C., De Velde, K., Morel, C., Capodaglio, G., Cescon, P., Scarponi, G., Boutron, C. 2001. Greenland Snow Evidence of Large Scale Atmospheric Contamination for Platinum, Palladium, and Rhodium. *Env. Sci. Technol.* Vol 35. 835-839.

Bekov, G., Letokhov, V., Radaev, V., Baturin, G., Egorov, A., Kursky, A., and Narseyev, V. 1984. Ruthenium in the ocean. *Nature.* Vol 312. 748-750.

Berner, R., Lasaga, A., and Garrels, R. 1983. The carbonate-silicate geochemical cycle and its effect on atmospheric carbon dioxide over the past 100 million years. *Amer. Jrnl. of Sci.* Vol 283. 641-683.

Birck, J., Roy Barman, M., and Capmas, F. 1997. Re-OsIsotopic Measurements at the Femtomole Level in Natural Samples. *Geostndrd. and geoanal.* Vol 20. 19-27.

Brandon A., Norman M., Walker R. and Morgan J. 1999. ^{186}Os-^{187}Os systematics of Hawaiian picrites. *Earth and Planetary Science Letters* Vol 174. 25-42.

Brügmann, G. and Naldrett, A. 1988. Platinum group element abundances in mafic and ultramafic rocks: Preliminary geochemical studies at the Lac des Iles complex, District of Thunder Bay, Ontario. Ont. Geo. Srvy. Opn. File Rpt. 5691. 43.

Brumsack, H. 1989. Geochemistry of recent TOC-rich sediments from the Gulf of California and the Black Sea. *Geol. Rundsch.* Vol 78. 851-882.

Brumsack, H. 2006. The trace metal content of recent organic carbon-rich sediments: Implications for Cretaceous black shale formation. *Paleogeo. Paleoclim. Paleoecol.* Vol 232. 344-361.

Byrne, H. 2002. Inorganic speciation of dissolved elements in seawater: the influence of pH on concentration ratios. *Geochem. Trans.* Vol 3. 11-16.

Byrne, R. and Yao, W. 2000. Formation of palladium(II) hydroxychloride complexes and precimitates in sodium chloride solutions and seawater. *Geochem. et Cosmochem. Acta.* Vol 64. 4153-4153.

Calvert, S. and Pedersen, T. 1993. Geochemistry of Recent oxic and anoxic marine sediments: Implications for the geological record. *Marin. Geo.* Vol 113. 67-88.

Chen, C. and Sharma, M. 2009. High Precision and High Sensitivity Measurements of Osmium in Seawater. *Anal. Chem.* Vol 81. 5400-5406.

Creaser, R., Papanastassiou, D., Wasserburg, G. 1991. Negative thermal ion mass spectrometry of osmium, rhenium, and iridium*. Geochem. et Cosmochem. Acta.* Vol 55. 391-401.

Cobelo-Garcia, A., Turner, A., Millward, G., and Couceiro, F. 2007. Behavior of palladium(II), platinum(IV), and rhodium(III) in artificialand natural waters: Influence of reactor surface and geochemistry on metal recovery. *Analytica chimica acta.* Vol 585. 202-210.

Cohen, A., Waters, F. 1996. Separation of osmium from geological materials by solvent extraction for analysis by thermal ionisation mass spectrometry*. Anal. Chem. Vol.* 332. 269-275.

Crocker, J., MacDougall, J., and Harriss, R. 1973. Palladium and iridium in marine sediments*. Geochem. et Cosmochem. Acta.* Vol 37. 2547-2556.

Donovan, A., Staerker, T., Pramudito, A., Li, W., Corbett, M., Lowery, C., Romero, A., Gardner, R. 2012. The Eagle Ford outcrops of West Texas: understanding heterogeneities within unconventional mudstone reservoirs. GCAGS J. 1. 162–185.

Du Vivier, A., Selby, D., Sageman, B., Jarvis, I., Grocke, D., and Voight, S. 2014. Marine 187Os/188Os stratigraphy reveals the interaction of volcanism and ocean circulation during Ocean Anoxic Event 2. *Erth. and Plntry. Sci. Ltrs.* Vol 389. 23-33.

Du Vivier, A., Jacobson, A., Lehn, G., Selby, D., Hurtgen, M., and Sageman, B. 2015-1. Ca isotope stratigraphy across the Cenomanian-Turonian OAE 2: Links between volcanism, seawater geochemistry, and the carbonate fractionation factor. *Erth. and Plntry. Sci. Ltrs.* Vol 416. 121-131.

Du Vivier, A., Selby, D., Condon, D., Takashima, R., and Nishi, H. 2015-2. Pacific $^{187}Os/^{188}Os$ isotope chemistry and U-Pb geochronology: Synchroneity of global Os isotope change across OAE 2. *Erth. and Plntry. Sci. Ltrs.* Vol 428. 204-216.

Dymond, J., Lyle, M., Finney, B., Piper, D., Murphy, K., Conrad, R., and Pisias, N. 1984. Ferromanganese nodules from MANOP Sites H, S, and R – control of mineralogical and chemical compositions by multiple accretionary processes. *Geochem. et Cosmochem. Acta.* Vol 48. 931-949.

Eary, L. and Rai, D. 1987. Kinetics of chromium (III) oxidation to chromium (VI) by reaction with manganese dioxide. *Env. Sci. Tech.* Vol 21. 1187-1193.

Elder, W. 1985. Biotic patterns across the Cenomanian-Turonian extinction boundary near Pueblo, Colorado (USA). *Geol. Soc. Am. Bull.* Vol. 106. 892 -902.

Ellis, A., Johnson, T., and Bullen, T. 2002. Chromium isotopes and the fate of hexavalent chromium in the environment. *Science*. Vol 295. 2060-2063.

Föllmi, K., Delamette, M. 1991. Model simulation of Mid-Cretaceous ocean circulation. *Science.* Vol 251. 94-95.

Francois, R. 1988. A study on the regulation of the concentrations of some trace metals (Rb, Sr, Zn, Pb, Cu, V, Cr, Ni, Mn, and Mo) in Saanich Inlet sediments, British Columbia, Canada. *Ma. Geo.* Vol 83. 285-308.

Frank, T. 2002. Radiogenic isotopes: tracers of past ocean circulation and erosional input. *Rev. Geophys.* Vol 40. 1-38.

Gale, A. and Christensen, W. 1996. Occurrence of the belemnite Actinocamax plenus in the Cenomanian of SE France and its significance. *Bull. Geol. Soc. Denmark.* Vol 43. 68-77.

Gammons, C. 1997. Experimental investigations of the hydrothermal geochemistry of platinum and passadium: V. Equilibria between platinum metals, Pt(II), and Pt(IV)

chloride complexes at 25 ro 300°C. *Geochem. et Cosmochem. Acta.* Vol 60. 1683-1694.

Goldberg, E. 1987. Comparative chemistry of the platinum and other heavy metals in the marine environment. *Pure and Appl. Chem.* Vol 59. 565-571.

Hild, E., and Brumsack, H. 1998. Major and Minor element geochemistry of Lower Aptian sediments from the NW German basin (core Hoheneggelsen KB 40). *Cretc. Res.* Vol 19. 615-633.

Hoernle, K., Hauff, F., and van den Bogaard, P. 2015. 70 m.y. history (139 - 69 Ma) for the Carribean large igneous province. *Geology.* Vol 32. 697-700.

Handoh, I. and Lenton, T. 2003. Periodic mid-Cretaceous oceanic anoxic events linked to oscillations of the phosphorous and oxygen biogeochemical cycles. *Glbl. Biogeochem. Cycls.* Vol 17. 1-11.

Hentz, T. and Ruppel S. 2010. Regional lithostratigraphy of the Eagle Ford shale: Maverick Basin to East Texas Basin. *Gulf Cst. Assc. of Geol Soc.* Vol 60. 325-337.

Hua, B., Deng, B., Thornton, E., Yang, J., and Amonette, J. 2007. Incorportation of chromate into calcium carbonate structure during coprecipitation. *Water Air Soil Pollut.* Vol 179. 381-390.

Huerta-Diaz, M., and Morse, J. 1992. Pyritisation of trace metals in anoxic marine sediments. *Geochim. Cosmochim. Acta* Vol 56. 2681-2702.

Jarvis, I., Lignum, J., Grocke, D., Jenkyns, H, Pearce, M. 2011. Black shale deposition, atmospheric CO_2 drawdown and cooling during the Cenomanian-Turonian Oceanic Anoxic Event. *Paleoocean.* Vol 26. 1-17.

Jenkyns, H. 2010. Geochemistry of oceanic anoxic events*. Geochem. Geophys. Geosys.* Vol 11. 1-30.

Jenkyns, H., Dickson, A., Ruhl, M., and Van Den Boorn, S. 2017. Basalt-seawater interaction, the Plenus Cold Event, enhanced weathering and geochemical change: deconstructing Oceanic Anoxic Event 2(Cenomanian-Turonian, Late Cretaceous). *Sedimentology* Vol 64. 16-43.

Keller, G. and Pardo, A. 2004. Age and paleoenvironment of the Cenomanian-Turonian global stratotype section and point at Pueblo, Colorado. *Marn. Mcroplntolgy.* Vol 51. 95-128.

Kendall, B., Creaser, R., and Selby, D. 2009. 187Re-187Os geochronology of Precambrian organic-rich sedimentary rocks. *Geol. Soc. Lndn Spec. Pub.* Vol 326. 85-107.

McDonough, W., and Sun, S. 1995. The composition of the Earth. *Chem. Geol.* Vol 120. 223-253.

Mondal, S. 2011. Platinum Group Element (PGE) Geochemistry to understand the Chemical Evolution of the Earth's Mantle. *Jrn. Geolog. Soc. Of India.* Vol 77. 295-302.

Monteiro, F., Pancost, R., Ridgwell, A., and Donnadieu, Y. 2012. Nutrients as the dominant contron on the spread of anoxia and euxinia across the Cenomanian-Turonian oceanic anoxic event (OAE2): Model-data comparison. *Paleocean.* Vol 27. 1-17.

Montgomery S., Petty A., and Post P. 2002. James Limestone, northeastern Gulf of Mexico: Refound opportunity in a Lower Cretaceous trend. *AAPG Bulletin* Vol 86. 381-397.

Morse, J. and Luther, G. 1999. Chemical influences on trace metal-sulfide interactions in anoxic sediments. *Geochem. et Cosmochem. Acta.* Vol 63. 3373-3378.

Naldrett S. and Libby W. 1(948) Natural radioactivity of rhenium. *Physics Review.* Vol 73. 487-493.

Orth, C., Attrep, M., Quintana, L., Elder, W., Kauffman, E., Diner, R., and Vilamil, T. 1993. Elemental abundance anomalies in the late Cenomanian extinction interval: A search for the source(s). *Earth and Planetary Science Letters.* Vol 117. 189-204.

Owens, J., Lyons, T., Li, X., MacLeod, K., Gordon, G., Kuypers, M., Anbar, A., Kuhnt, W., and Severmann, S. 2012. Iron isotope and trace metal records of iron cycling in the proto-North Atlantic during the Cenomanian Turonian oceanic anoxic event (OAE-2). *Paleocean.* Vol 27. 1-13.

Oxburgh, R. 2001. Residence time of osmium in the oceans. *Geochem. Geophys. Geosyst.* Vol 2. 1-17.

Peucker-Ehrenbrink and G., Ravizza. 2000. The marine Os isotope record. *Terra-Nova.* Vol 12. 205-219.

Peucker-Ehrenbrink, G., Ravizza, G., Hofmann, A. 1995. The marine ^{187}0s/ ^{186}0s record of the past 80 million years. *Earth and Planetary Science Letters* Vol 130. 155-167.

Pessagno, A. 1969. Upper Cretaceous stratigraphy of the western Gulf Coast area of Mexico, Texas, and Arkansas. *In Memoir – GSA.* Vol 111. 1-139.

Pindell J., Cande S., Pitman W., Rowley D., Dewey J., LaBreeque, J. and Haxby, W. 1988. A plate-kinematic framework for models of Caribbean evolution. *Tectonophysics* Vol 155. 121-139.

Pogge von Strandmann, P., Jenkyns, H., and Woodfine, R. 2013. Lithium isotope evidence for enhanced weathering during Oceanic Anoxic Event 2. *Nat. Geosci.* Vol 6. 668-672.

Pratt, L. and Davis, D. 1992. Intertwined fates of metals, sulfur, and organic carbon in black shales. *SEPM Shrt. Crse* Vol 27. 1-27.

Puchtel, I. Platinum Group Elements. *Encyclopedia of Geochemistry*. DOI: 10.1007/978-3-319-39193-9_274-1.

Rauch, S. and Morrison, G. 2008. Environmental relevance of the platinum-group elements. *Elements* Vol 4. 259-263.

Ravizza, G. and Pyle, D. 1997. PGE and Os isotopic analyses of simple sample aliquots with NiS fire assay preconcentration. *Chem. Geo.* Vol 141. 251-268.

Rose P.R. (1972) Edwards Group, surface and subsurface, central Texas. *UT Austin Bur. of Econmc. Geo. Rep. of Invstgn* Vol 74. 198.

Saito, M., Moffett, J., Chisholm, S. and Waterbury, J. 2002. Cobalt limitation and uptake in Prochlococcus. Limnol. *Oceanogr.* Vol 47. 1629-1636.

Salvador, A. 1991. Origin and development of The Gulf of Mexico Basin. Boulder, Colorado, Geological Society of America, The Geology of North America. 389-444

Salvador, A. and Muneton, J. 1989. Stratigraphic Correlation Chart Gulf of Mexico Basin, The Gulf of Mexico Basin: Boulder Colorado Geological Society of America, The Geol. of North America, V. J., Plate 5.

Scheiderich, K., Amini, M., Holmde, C., and Francois, R. 2015. Global variability of chromium isotopes in seawater demonstrated by Pacific Atlantic and Arctic Ocean samples. *Erth. And Plntry. Sci. Ltr.* Vol 423. 87-97.

Schlanger, S., Arthur, M., Jenkyns, H. and Scholle, P. 1987. The Cenomanian-Turonian oceanic anoxic event, I. Stratigraphy and distribution of organic carbon-rich beds and the marine δ13C excursion. *Marn. Petr. Sorc. Rocks.* Vol 26. 371-399.

Schlanger, S. and Jenkyns, H. 1976. Cretaceous Oceanic Anoxic Events: Causes and Consequences. *Netherlands Jrnl. of Geosci.* Vol 55. 179-184.

Scopelliti, G., Bellance, A., Neri, R., Coccioni, R. 2006. Comparitive high-resolution chemostratigraphy of the Bonarelli Level from the reference Bottaccione section (Umbria-Marche Apennines) and from an equivalent section in NW Sicily: Consistent and contrasting responses to the OAE2. *Chem. Geo.* Vol 228. 266-285.

Scott R. 1993. Cretaceous carbonate platform, U.S. Gulf coast. *In: Simo J.A., Scott R.W. and Masse J.P. (Eds.), Cretaceous Carb. Platforms, AAPG Memoir* Vol 56. 97-109.

Selby, D., Creaser, R. 2003. Re–Os geochronology of organic rich sediments: an evaluation of organic matter analysis methods. *Chem. Geol.* Vol 200. 225–240.

Selby, D., Creaser, R., Stein, H., Markey, R., and Hannah, J. 2007. Assessment of the ^{187}Re decay constant by cross calibration of Re-Os molybdenite and U-Pb zircon chronometers in magmatic ore systems. *Geochem. et Cosmochem. Acta.* Vol 71. 1999-2013.

Sharma, M., Rosenberg, E., and Butterfirld, D. 2007. Search for the proverbial mantle osmium sources to the oceans: Hydrothermal alteration of mid-ocaen ridge basalt. *Geochem. et Cosmochem. Acta.* Vol 71. 4655-4667.

Sharma, M and Wasserburg, G. 1997. Osmium in the rivers. *Geochem. et Cosmochem. Acta.* Vol 61. 5411-5416.

Sikora, E., Johnson, T., and Bulled, T. 2008. Microbial mass-dependant fractionation of chromium isotopes. *Geochem. et Cosmochem. Acta.* Vol 72. 3631-3641.

Sinton, C. and Duncan, R. 1997. Potential links between ocean basalt volcanism and global ocean anoxia at the Cenomanian-Turonian boundary. *Econ. Geol.* Vol 92. 836-842.

Smoliar, S., Walker, R., and Morgan, J. 1996. Re-Os isotope constraints on the age of Group IIA, IIIA, IVA, and IVB iron meteorites. *Science* Vol 271. 1099-1102.

Snow, L., Duncan, R., and Bralower, T. 2005. Trace element abundances in the Rock Canyon Anticline, Pueblo, Colorado, marine sedimentary section and their relationship to Carribean plateau construction and oxygen anoxic event 2. *Paleoceanography* Vol 20. 1-14.

Tang, Y., Elzinga, E., Jae Lee, Y., and Reeder, R. 2007. Coprecipitation of chromate with calcite: Batch experiments and X-Ray absorption spectroscopy. *Geochem. et Cosmochem. Acta.* Vol 71. 1480-1493.

Taylor, S., and McLennan, S. 1985. The continental crust: its composition and evolution. *Blackwell, Oxford.* 312 pages.

Tribovillard, N., Algeo, T., Lyons, T., and Riboulleau, A. 2006. Trace metals as paleoredox and paleoproductivity proxies: An update. *Chem. Geo.* Vol. 232. 12-32.

Volkening, J., Walczyk, T., Heumann, K. 1991. Osmium isotope ratio determinations by negative thermal ionization mass spectrometry. *Int. Journal of Mass Spectrometry and Ion Processes.* Vol. 105. 147-159.

Whitfield, M. 2002. Interactions between phytoplankton and trace metals in the ocean. *Adv. Mar. Biol.* Vol 41. 3-120.

Widom, E. and Shirey, S. 1996. Os isotope systematics in the Azores: implications for mantle plume sources. *Earth and Planetary Science Letters* Vol 142. 451-465.

Wright, S.W. 2015. University of Houston PhD thesis chapter 3. Department of Earth and Atmospheric Sciences.

Yamashita, Y., Takahashi, Y., Haba, H., Enomoto, S., and Shimizu, H. 2007. Comparison of reductive accumulation of Re and Os in seawater-sediment systems. *Geochem. et Cosmochem. Acta.* Vol 71. 3458-3475.

Yang, G., Zimmerman, A., Stein, H., and Hannah, J. 2015. Pretreatment of nitric acid with hydrogen peroxide reduces total procedural Os blank to femtogram levels. *Anal. Chem*. Vol 87. 7017-7021.

Yurewicz D.A., Marler T.B., Meyerholtz K.A. and Siroky F.X. (1993) Early Cretaceous carbonate platform, north rim of the Gulf of Mexico, Mississippi and Louisiana. *In: Simo J.A., Scott R.W. and Masse J.P. (Eds.), Cretaceous Carb. Platforms, AAPG Memoir* Vol 56. 81-96.

Zhou, X., Jenkyns, H., Owens, J., Junium, C., Zheng, X., Sageman, B., Hardisty, D., Lyons, T., Ridgwell, A., and Lu, Z. 2015 Upper ocean oxygenation dynamics from I/Ca ratios during Cenomanian-Turonian OAE 2. *Paleoceanography* Vol. 510-526.